BIOMATERIALS

Rapid closure and hemostasis of ruptured soft tissues using a modified human tropoelastin-based sealant in preclinical models

Mahsa Ghovvati^{1,2}†, Saumya Jain¹†, George Z. Cheng³, Naoki Kaneko², Joshua A. Boys⁴, Taichiro Imahori², Tess De Maeseneer¹, Reihaneh Haghniaz⁵, Robert B. Cameron^{6,7}, Anthony S. Weiss^{8,9,10}, Nasim Annabi^{1,11}*

Treatment of injuries to soft elastic organs is often hindered by challenging anatomical features and limitations of existing sealant materials, which may lack adequate tissue adhesion, elasticity, biocompatibility, and effective hemostatic properties. To address these clinical challenges, we developed an injectable elastic sealant formulated with methacryloyl-modified human recombinant tropoelastin (MeTro) and Laponite silicate nanoplatelets (SNs). We optimized the hydrogel formulation for mechanical properties, adhesion, biocompatibility, and hemostatic properties and used visible light for cross-linking to improve safety. MeTro/SN hydrogels had increased tissue adhesion strength and burst pressure in vitro and ex vivo compared with MeTro alone or commercial sealants. The addition of SNs to the hydrogels facilitated faster blood clotting in vitro without increasing hemolysis. Applied to incisional injuries on rat lungs or aortas, MeTro/SN had burst pressures comparable to those of native tissue and greater than those of MeTro after a 7-day in vivo application. On porcine lungs, MeTro/SN also supported effective lung sealing and burst pressure similar to native lung 14 days after injury sealing. In a rodent tail hemostasis model, MeTro/SN reduced bleeding compared with MeTro. In an injured porcine lung model, early hemostasis was better than the tested commercial sealants. The results demonstrated that MeTro/SN provided effective tissue sealing and promoted hemostasis in a time frame that minimized blood loss without causing a major inflammatory response. These findings highlight the translational potential of our engineered sealant with biomimetic mechanics, durable tissue adhesion, and rapid hemostasis as a multipronged approach for the sealing and repair of traumatic injuries to soft organs.

Copyright © 2025 The Authors, some rights reserved; exclusive licensee American Association for the Advancement of Science. No claim to original U.S. Government Works

INTRODUCTION

Traditional methods of surgical wound closure include sutures, wires, and staples that require tissue mechanical compliance and are often inappropriate for application on highly elastic soft tissues such as the lung, heart, muscle, and blood vessels. These methods also do not address the issue of hemorrhage that often accompanies traumatic injuries, leading to prolonged surgical treatment and necessitating blood transfusions. Therefore, hemostatic sealants have been developed to reduce chances of wound dehiscence and blood loss (1-4). These multifunctional materials require robust adhesion for wound closure and effective mechanisms for quick hemostasis (1). However, most commercially available surgical sealants (Dermabond, Coseal, and Progel) fail to provide both properties simultaneously (5). Others that are capable of hemostatic sealing (Floseal, SurgiFlo, and Tisseel)

¹Department of Chemical and Biomolecular Engineering, University of California, Los Angeles, Los Angeles, CA 90095, USA. ²Department of Radiological Sciences, David Geffen School of Medicine, University of California, Los Angeles, Los Angeles, CA 90095, USA. ³Division of Pulmonary, Critical Care, and Sleep Medicine, University of California, San Diego, La Jolla, CA 92093, USA. ⁴Division of Cardiothoracic Surgery, Department of Surgery, University of California, San Diego, La Jolla, CA 92093, USA. ⁵Terasaki Institute for Biomedical Innovation (TIBI), Los Angeles, CA 90024, USA. $^6\mathrm{Division}$ of Thoracic Surgery, Department of Surgery, David Geffen School of Medicine at UCLA, Los Angeles, CA 90095, USA. ⁷Division of Thoracic Surgery, Department of Surgery and Perioperative Care, West Los Angeles VA Medical Center, Los Angeles, CA 90095, USA. 8Charles Perkins Centre, University of Sydney, Camperdown, NSW 2006, Australia. 9School of Life and Environmental Sciences, University of Sydney, Camperdown, NSW 2006, Australia. ¹⁰Sydney Nano Institute, University of Sydney, Camperdown, NSW 2006, Australia. 11 Department of Bioengineering, University of California, Los Angeles, Los Angeles, CA 90095, USA. †These authors contributed equally to this work.

*Corresponding author. Email: nannabi@ucla.edu

incorporate gelatin or fibrin as a sealing matrix and thrombin or coagulating factors to promote hemostasis. Such hemostatic agents rely on the innate coagulatory response of the patient, which might be compromised in certain cases, and they may activate strong coagulation activators that can cause other medical problems (6, 7).

Commercial sealants are hindered by several limitations including low elasticity, stiffness, and tissue adhesion, particularly in wet and dynamic physiological environments. For example, cyanoacrylates enable strong adhesion but also high stiffness in the gigapascal range that is incompatible with native tissues and often presents cytotoxicity issues (8, 9). Alternatively, natural polymer-based sealants are biocompatible, but most have low mechanical properties and poor adhesion to wet, soft, or elastic tissues (10), which can prevent healthy tissue movement (11, 12). Sealants for lungs must withstand high pressures and deformation stress while retaining durable mechanoadhesive properties. Commercial lung sealants such as poly(ethylene glycol)-based FocalSeal (a discontinued product) and Progel have usability issues such as prolonged application time or necessity for sutures to remain in place (13–15). Therefore, there is still a need for a sealant that combines adequate mechanical flexibility and compliance without sacrificing strength and adhesion suitable for application on soft elastic tissues.

We explored the use of modified recombinant human tropoelastin for lung sealing because it mimics native elastin and has relevance in the realm of elastic tissue engineering (16-21). Our group previously developed methacryloyl-substituted tropoelastin (MeTro) to seal elastic tissues such as lungs and arteries (22). A natural MeTro polymer enables biocompatibility and also provides mechanical properties that are mimetic to those of native soft and elastic tissues, which can facilitate biological cues necessary for tissue regeneration and repair after an injury (23). We have also modified MeTro with graphene oxide (GO) to impart conductivity and enhance toughness (16), and to treat peripheral nerve injury, we combined MeTro with methacryloyl-modified gelatin (GelMA) (20). Herein, we sought to adapt this material system for treating hemorrhagic wounds with the goal of producing a surgical sealant that minimizes blood loss and mitigates the need for transfusions during traumatic bleeding incidents. We combined MeTro with varying amounts of silicate nanoplatelets (SNs), which provided a straightforward and easily scalable method to enhance the hemostatic properties of the resulting hydrogel (24, 25). The SN nanoclay has demonstrated hemostatic activity through electrostatic interactions between its charged surfaces and blood cells as well as by concentrating clotting factors (26–28). Recently, a commercial SN (Laponite)-loaded hydrogel was approved by the US Food and Drug Administration for use as a vascular embolization device (29). Although Laponite-containing hydrogels have been explored for mechanical reinforcement or hemostasis, their applicability in sealing dynamic soft tissues remains limited. Given the need for a material that provides both structural stability and hemostatic function, we sought to integrate Laponite with MeTro.

In this study, we focus on overcoming the current drawbacks of hemostatic sealants by engineering a multifunctional hydrogel that exhibits high elasticity, strong adhesion to wet tissue, hemostatic properties, and biocompatibility. We first characterized the prepolymer and hydrogel with proton nuclear magnetic resonance (¹H NMR) spectroscopy and optimized the physical and mechanical properties by varying SN concentrations. The tissue adhesion ability was monitored using in vitro and ex vivo adhesion and burst pressure tests on various mammalian tissues (skin, lungs, and heart) and compared with commercial sealants. In vitro hemostasis with fresh human whole blood and in vitro biocompatibility with two-dimensional (2D) seeded human lung fibroblast (hLFB) cells were tested directly on the hydrogels. Biocompatibility and biodegradability were further monitored in vivo using rat subcutaneous implantation. In vivo burst pressure was tested on incised rat lungs and aortas that were sealed for 7 days as well as on pig lung lacerations that were sealed for 14 days with MeTro, MeTro/SN, or commercial controls. In vivo hemostatic properties of the engineered hydrogels were also assessed using rat tail amputation and pig lung laceration models and compared with commercial controls. The host immune response was evaluated on tissue surrounding the sealants after the implantation period. Our findings from these studies emphasize the translational relevance of the MeTro/SN hemostatic sealant for hemorrhage control and wound treatment in urgent clinical settings.

RESULTS

Synthesis and characterization of MeTro/SN hydrogels

A nanocomposite hydrogel was tailored for the air-tight hemostatic sealing of ruptured soft tissues through the synthesis of MeTro, synergistic introduction of SNs, and optimization of mechanical, adhesion, and hemostatic properties (Fig. 1A). Laponite, a commercially available SN, was used for its unique charge distribution, with a permanent negative charge on its outer oxygen-dense trioctahedral sheet and a positive charge on its inner magnesium oxide octahedral sheet (30). Prepolymer solutions of MeTro with varying amounts of SN were prepared in a lithium phenyl-2,4,6-trimethylbenzoylphosphinate (LAP) photoinitiator solution (31). LAP can be activated at 395 to

405 nm and does not require ultraviolet (UV) light exposure like other photocrosslinkers, which is an advantage for the safety and usability of the material. However, LAP concentrations above 0.5% (w/v) can be cytotoxic (32), so we used a concentration of 0.03% (w/v) LAP for the formation of the MeTro/SN hydrogels. The liquid composite hydrogel precursor could be photopolymerized after a short exposure to visible light. The possible chemical interactions cross-linking the hydrogel include ionic interactions between the magnesium (Mg²⁺) or lithium (Li⁺) ions within SNs and the carboxyl groups of MeTro; hydrogen bonds among different moieties on MeTro, such as amine or hydroxyl groups, or between MeTro and epoxides on SNs; covalent C—C bonds formed by the methacrylate components of MeTro; and electrostatic interactions between the charged surfaces of SNs and MeTro (Fig. 1B) (16).

We characterized the physical properties of the resulting hydrogel to confirm the incorporation of SNs into MeTro/SN hydrogels and to understand the potential interactions responsible for hydrogel formation. SNs are reported to exhibit negative zeta potential in both acidic and basic environments because of the abundance of anionic surface charge arising not only from the release of sodium ions in aqueous solution but also from the isomorphic replacement of Mg²⁺ with Li⁺ in the SN interlayer (33). Accordingly, the zeta potential of pure MeTro prepolymer solution (22 \pm 0.35 mV) decreased to 20 ± 0.31 mV after the addition of 1% (w/v) SN (Fig. 1C), indicating a potential for electrostatic interactions between the hydrogel constituents. Pure MeTro hydrogels showed a swelling ratio of $16 \pm 0.81\%$ within 72 hours of incubation in Dulbecco's phosphate-buffered saline (DPBS) solution. However, increasing the SN content to 1 and 1.5% (w/v) enhanced the swelling ratio of the composites to 21 ± 1.3 (P < 0.05) and $25 \pm 1.2\%$ (P < 0.0001), respectively, during the same incubation period (Fig. 1D), which may be due to infiltration of water into the highly charged interlayers of SNs (30).

¹H NMR analysis of the prepolymers and cross-linked hydrogels was performed to confirm the chemical identity of the modified biopolymers. To synthesize MeTro, pure tropoelastin was modified with methacrylic anhydride (MA), which resulted in the appearance of two vinylic proton peaks at 5.84 and 6.16 ppm (parts per million) (Fig. 1E). The addition of SNs to the prepolymer had no effect on the ¹H NMR spectra of MeTro. After photocrosslinking of the MeTro/ SN prepolymer, the vinyl proton peaks disappeared because of their contribution to the formation of the C—C covalent bonded network. The degree of cross-linking was then calculated as the percentage difference in area under the vinylic proton peaks in the prepolymer and hydrogel samples. The pure MeTro hydrogel showed an 89% degree of cross-linking, whereas MeTro/SN hydrogels containing 0.5, 1, and 1.5% (w/v) SN had cross-linking degrees of 88, 80, and 80%, respectively. The degree of methacrylation of MeTro was also assessed using ¹H NMR. The percentage difference in area under the lysine proton peak (at 2.74 ppm, blue-shaded area) for pure tropoelastin and MeTro prepolymer revealed that the latter had a 94% degree of methacrylation (Fig. 1E).

Bonding interactions within the cross-linked hydrogels were further analyzed with Fourier transform infrared spectroscopy. Both MeTro and MeTro/SN [containing 1% (w/v) SN] hydrogels exhibited broad peaks around 3200 to 3600 cm⁻¹, indicating O—H and N—H stretching vibrations (fig. S1) (34). Because of their low transmittance, there are likely hydrogen bonding interactions between hydroxyl/amino groups and other electronegative moieties on the MeTro polymer. Furthermore, we noted lower transmittance in

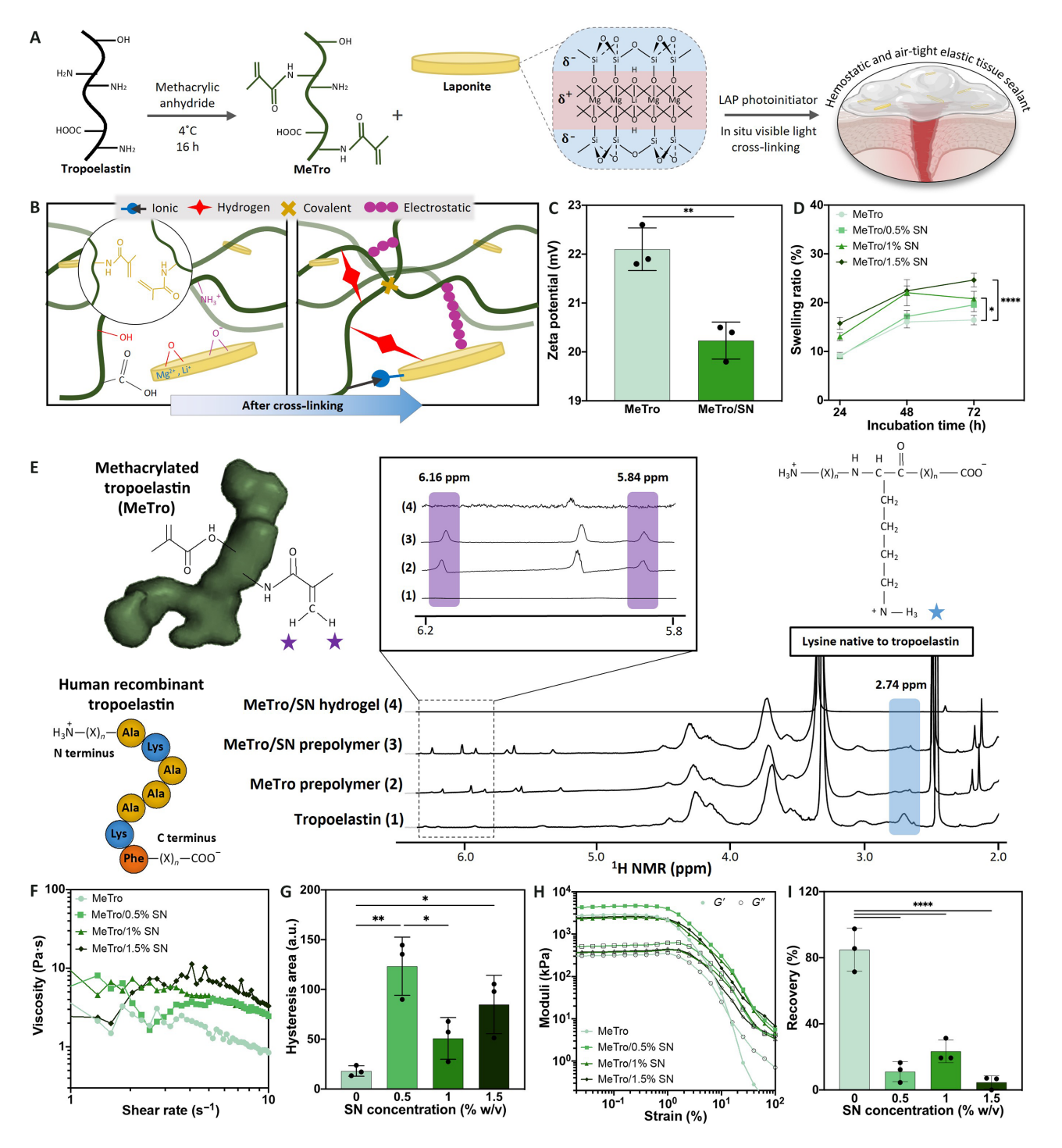


Fig. 1. Synthesis and physical characterization of MeTro/SN hydrogels that exhibited thixotropic properties with higher SN concentration. (A) Schematic of the synthesis of MeTro and combination with SN to produce the MeTro/SN hydrogel that can provide hemostatic and air-tight sealing of elastic tissue. h, hours. (B) Schematic of molecular interactions between MeTro and SN with cross-linking. (C) Zeta potential of MeTro and MeTro/SN [1% (w/v) SN] prepolymer solutions. Analysis by unpaired two-tailed Student's t test. n = 3. (D) In vitro swelling behavior of MeTro/SN hydrogels with various concentrations of SN [0, 0.5, 1, and 1.5% (w/v)] in DPBS. n = 3. (E) Schematic representation of MeTro and tropoelastin (left) and ¹H NMR spectra of tropoelastin (1), MeTro prepolymer (2), MeTro/SN [1% (w/v) SN] prepolymer (3), and MeTro/SN [1% (w/v) SN] hydrogel (4). Purple, methacryloyl protons on MeTro and MeTro/SN; blue, amine protons on lysine residues on the backbone of the tropoelastin peptide [abbreviated as (X)_n]. (F) Viscosity of MeTro and MeTro/SN prepolymer solutions. Representative of n = 3. (G) Hysteresis area or measure of thixotropy of MeTro/SN prepolymer solutions. a.u., arbitrary units. (H) Strain sweep of MeTro/SN prepolymer solutions containing various concentrations of SN [0, 0.5, 1, and 1.5% (w/v)] at a constant frequency of 10 rad/s. Representative of n = 3. (I) Recovery percentage of MeTro/SN hydrogels containing various concentrations of SN [0, 0.5, 1, and 1.5% (w/v)] after three breakdown/recovery cycles. Data in (C), (D), (G), and (I) are presented as the means \pm SD; dots represent individual samples. Analysis in (D), (G), and (I) by one-way ANOVA with Tukey's post hoc multiple comparisons test. For all panels, n = 3. *P < 0.05, *P < 0.05, *P < 0.00, and *P < 0.00. Illustrations created with BioRender.

MeTro/SN samples (compared with the pure MeTro hydrogel) around 2800 to 3000 cm⁻¹, a region that typically represents C—H stretching, which could denote van der Waals interactions between MeTro methyl groups and SN silicate groups (35). Furthermore, the peak at 1931 cm⁻¹ in the MeTro/SN spectrum could signify metal-carbonyl complexation, which further demonstrates SN interactions with the MeTro polymer.

The incorporation of SN is known to increase viscosity at low shear rates and to impart thixotropy, or time-dependent shearthinning properties, to prepolymer solutions and hydrogels (35). Therefore, we evaluated the rotational rheological behavior of the prepolymer solutions and the oscillatory rheological response of the cross-linked hydrogels that were prepared with different concentrations of SNs. As expected, there was a change in the viscosity of MeTro and MeTro/SN prepolymers over different shear rates (Fig. 1F). The viscosity of the pure MeTro prepolymer (1.0 \pm 0.36 Pa·s) was significantly lower than that of MeTro/SN containing 1.5% (w/v) SN (3.0 \pm 0.44 Pa·s) (P < 0.01) (fig. S2A). Higher viscosity is desirable to ensure that the polymer precursor stays in its applied region over an injury without flowing into off-target surrounding areas before photocrosslinking. The thixotropic properties of the prepolymer solutions were assessed by quantifying the hysteresis area between the up-ramp (increasing shear rate) and the downramp (decreasing shear rate) in rotational measurements. The pure MeTro precursor depicted almost no hysteresis, whereas the SNcontaining prepolymer solution showed more distinct signs of hysteresis (fig. S2B). The hysteresis area of pure MeTro was lower than that of MeTro/SN containing 1.5% (w/v) SN (P < 0.05), whereas solutions with 0.5% (w/v) SN exhibited a significantly higher hysteresis area than those with either 0% (w/v) SN (P < 0.01) or 1% (w/v) SN (P < 0.05) (Fig. 1G). A certain amount of thixotropy is desirable because it allows the solution to be easily injected but still recover after application. However, too much thixotropy means that the sample will take a long time to recover, and wound sealing typically needs to occur quickly. Therefore, MeTro/SN solutions with 1 and 1.5% (w/v) SN show more favorable behavior than the solution with 0.5% (w/v) SN. We also evaluated the thixotropic behavior of the cross-linked hydrogels by alternating cycles of hydrogel breakdown and recovery, during which all samples showed a gel character with G' > G'' up to 1% strain (Fig. 1H). Therefore, we assessed the elastic modulus of each MeTro/SN formulation when 50% strain was applied to break down the hydrogel and 0.1% strain was applied for recovery (fig. S2C). Hydrogels containing SNs showed lower recovery compared with pure MeTro (P < 0.0001), which confirmed that the presence of the nanoplatelets imparted thixotropic character to the engineered MeTro/SN hydrogels (Fig. 1I). The relatively slow initial recovery could be due to the large number of reversible interactions that need to reform, and it could permit the hydrogel to be injected as well as to adapt to diverse tissue terrains and dynamic organ movement.

MeTro/SN hydrogels exhibit improved physical properties compared with MeTro and commercial sealants

Biomaterial-based sealants for wound closure should support the mechanical motion required by the injured tissue structures. Therefore, we evaluated the mechanical properties of our engineered MeTro/SN hydrogels through tensile and compression testing. The duration of visible light exposure required to fully cross-link the MeTro hydrogels was optimized using compression tests, which revealed that 40 s of

light exposure caused the hydrogel to have a compression Young's modulus of 9.0 ± 1.4 kPa, whereas exposure for 80 s caused a modulus of 13 ± 1.0 kPa (fig. S3). After 80 s of complete photocrosslinking, the pure MeTro hydrogel exhibited an ultimate strength of 29 ± 8.2 kPa (Fig. 2A). When SN was introduced, the strength of the samples containing 0.5% (w/v) SN (21 ± 4.5 kPa) was significantly enhanced in the samples containing 1% (w/v) SN (41 \pm 4.4 kPa, P < 0.05) or 1.5% (w/v) SN (42 \pm 3.6 kPa, P < 0.01). The increase in ultimate strength of the nanocomposites could be attributed to the incorporation of nanoclays, which not only introduced an element of rigidity but also provided a means of noncovalent interactions with MeTro polymers, thereby strengthening the matrix (36). Furthermore, increasing the amounts of SNs did not compromise the tensile Young's modulus, extensibility (fig. S4), or compressive modulus (fig. S5) of the MeTro/ SN hydrogels. The abundance of reversible noncovalent interactions in the MeTro/SN network could also permit energy dissipation upon deformations, such as those during cyclic compression tests (Fig. 2B). Because of this phenomenon, after five compression cycles, the energy loss experienced by MeTro/SN with 1.5% (w/v) SN (16 \pm 2.2%) was higher than that by pure MeTro $(9.5 \pm 4.0\%)$ (P < 0.05) (Fig. 2C). We also analyzed the conductivity of the engineered composites to assess their capacity for supporting cellular communication by enabling electrical signaling through ion movements, which can coordinate cellular activities and affect wound healing (37). The pure MeTro hydrogel provided an ionic conductivity of 0.07 ± 0.006 S/m, whereas the MeTro/SN hydrogel containing 1% (w/v) SN had a higher conductivity of 0.09 ± 0.003 S/m (P < 0.05) (Fig. 2D).

MeTro/SN hydrogels exhibit strong adhesion on mammalian tissues compared with commercial sealants

Tissue sealants must exhibit not only strong mechanics but also robust tissue adhesion to withstand the dynamic motion that accompanies physiological activity. Therefore, the adhesive properties of the engineered MeTro/SN hydrogels were quantified both in vitro and ex vivo. In vitro wound closure adhesion was conducted on different types of porcine tissues including skin, lung, and heart. We did not observe a difference in adhesion between MeTro and MeTro/ SN on porcine skin; however, on lung tissue, the adhesion strength of the pure MeTro hydrogel (12 ± 2.8 kPa) was less than that of MeTro/SN with 1% (w/v) SN (23 \pm 0.85 kPa) (P < 0.01) (Fig. 2E). The MeTro/SN sealant exhibited a higher adhesion strength (16 ± 0.05 kPa) compared with the pure MeTro hydrogel (7.8 \pm 0.03 kPa) on heart tissue as well (P < 0.01) (Fig. 2E). The adhesion energy of the nanocomposite hydrogels was also higher compared with that of pure MeTro gels on skin tissue $(5.2 \pm 0.44 \text{ J/m}^2 \text{ versus } 2.9 \pm 0.43 \text{ J/m}^2)$ m^2 , P < 0.05) and on lung tissue (9.6 ± 1.1 J/m² versus 3.0 ± 2.0 J/ m^2 , P < 0.05) but not on heart tissue (Fig. 2F).

To test burst pressure, hydrogels were used to seal punctured and pressurized skin-mimicking collagen sheets. The pure MeTro hydrogel burst after the application of a pressure of 7.2 ± 0.77 kPa, whereas MeTro/SN with 1 and 1.5% (w/v) SN burst at significantly higher pressures (14 ± 0.41 and 14 ± 0.64 kPa, respectively) (P < 0.0001) (Fig. 2G). All engineered MeTro/SN formulations exhibited higher burst pressures than commercially used, biomaterial-based sealants including Evicel (3.7 ± 1.1 kPa), Coseal (1.7 ± 0.03 kPa), and Progel (4.1 ± 0.64 kPa) (P < 0.0001) (Fig. 2G). The SN-containing hydrogels showed increased adhesive properties compared with the pure MeTro gel because the nanoclays permit even more avenues for tissue interactions, including electrostatic, hydrogen, covalent, and

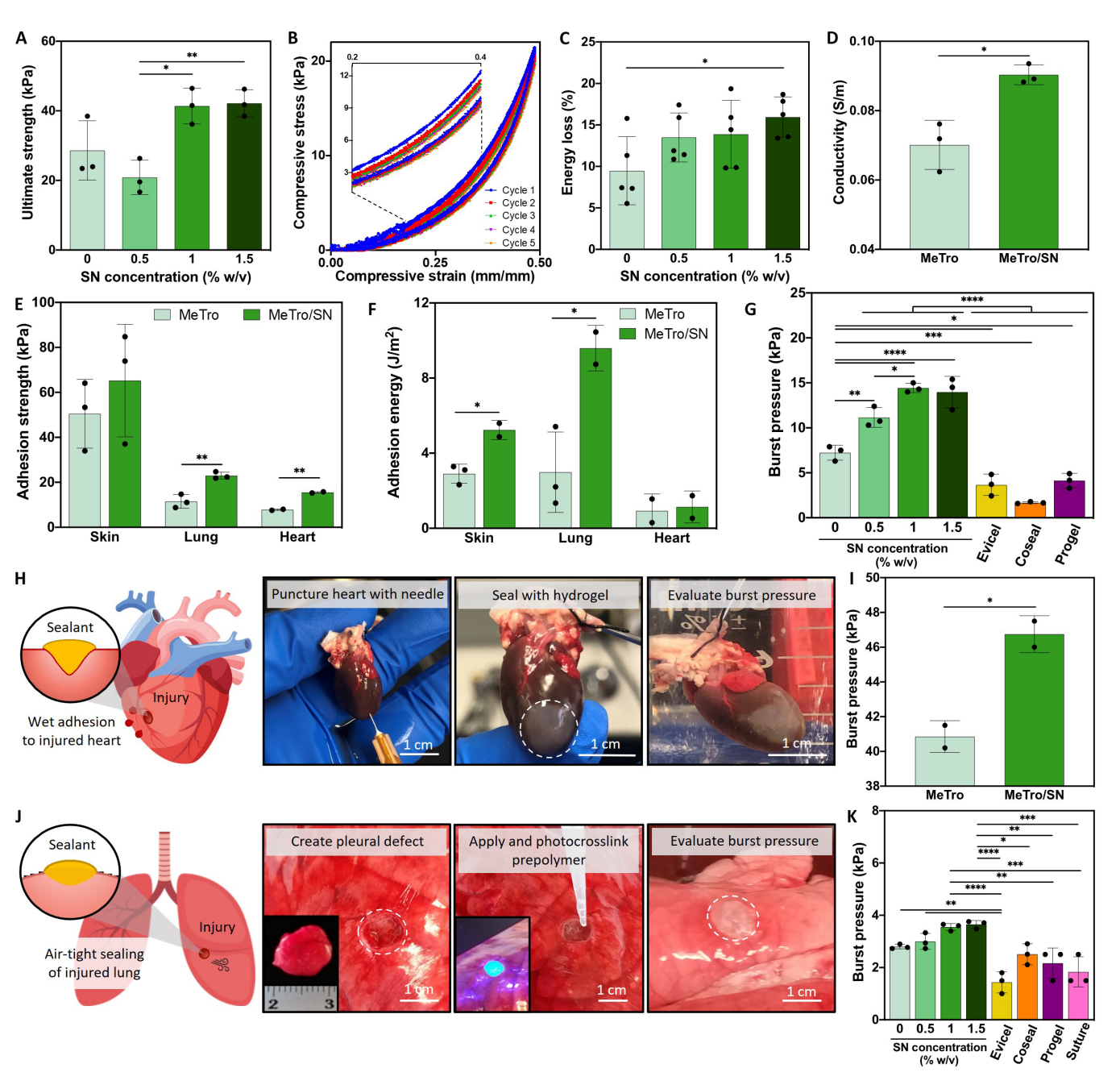


Fig. 2. MeTro/SN hydrogels exhibit increased physical and adhesive properties compared with MeTro and commercial sealants. (A) Ultimate strength of MeTro/SN hydrogels. n=3. (B) Cyclic compression strain-stress curves (five cycles) of MeTro/SN hydrogels containing 1% (w/v) SN. Representative of n=5. (C) Energy loss of MeTro or MeTro/SN hydrogels. n=5. (D) Conductivity of pure MeTro and MeTro/SN [1% (w/v) SN] hydrogels. Analysis by unpaired two-tailed Student's t test. n=3. (E) Adhesion strength and (F) adhesion energy of pure MeTro and MeTro/SN [1% (w/v) SN] hydrogels on different porcine tissues. Analysis by unpaired two-tailed Student's t test for each tissue. Skin, n=3; lung, n=3; heart, n=2. (G) In vitro burst pressure of MeTro/SN hydrogels compared with Evicel, Coseal, and Progel (22). n=3. (H) Schematic of the sealant applied to a heart puncture wound and images of the procedure and ex vivo burst pressure evaluation of pure MeTro and MeTro/SN [1% (w/v) SN] hydrogels from punctured and sealed explanted rat hearts. (I) Quantification of burst pressure. Analysis by unpaired two-tailed Student's t test. n=2. (J) Schematic and images of the sealant applied to a 1-cm pleural defect model on ventilated pig lungs. Lungs were sealed with MeTro/SN hydrogels, Coseal (12), Evicel, Progel, or suture (22). (K) Quantification of ex vivo burst pressure test. n=3. Data in (A), (C) to (F), (H), and (I) are presented as the means \pm SD; dots represent individual samples. Analysis in (A), (C), (G), and (K) by one-way ANOVA with Tukey's post hoc multiple comparisons test. *P < 0.05, **P < 0.01, ***P < 0.001, and ****P < 0.0001. Scale bars, 1 cm. Illustrations created with BioRender.

Downloaded from https://www.science.org at University of California Los Angeles on May 21, 2025

ionic bonds (fig. S6). Representative scanning electron microscopy images of the surfaces of MeTro (fig. S7A) or MeTro/SN (fig. S7B) hydrogels show that MeTro/SN hydrogels appeared to have more textured surfaces. Scanning electron microscopy imaging of both the interface of MeTro or MeTro/SN hydrogels and porcine lung tissues showed tissue interaction, supporting their potential for robust adhesion (fig. S7, C and D). The attachment was visible as a distinct interconnecting layer between the uniform hydrogel and the textured tissue. Both MeTro and MeTro/SN sealants appeared to conform to irregularities on the lung tissue surface, supporting a tight interaction between the hydrogel and tissue that would enable interaction with irregularly shaped wounds.

To further evaluate the adhesive properties of our engineered composites, we conducted ex vivo burst pressure tests on freshly isolated rat hearts and pig lungs using pure MeTro and MeTro/SN hydrogels as well as several commercial sealants for vascular and pleural reconstruction (Evicel, Coseal, and Progel). After the heart was confirmed to be free of leaks or injuries, it was punctured with a 15-G needle, and either MeTro or MeTro/SN prepolymers were photocrosslinked over the injury to form hydrogel sealants (Fig. 2H). The sealed heart was then subjected to increasing catheterdelivered pressure, and the burst pressure was monitored by aqueous submersion. The MeTro hydrogel burst upon application of a pressure of 41 \pm 0.72 kPa to the heart, whereas the MeTro/SN sealant burst at 47 ± 0.62 kPa (P < 0.05) (Fig. 2I). To test the hydrogel sealing capacity on ex vivo lung tissue, a 1-cm² pleural injury was created on explanted porcine lungs that were sealed with hydrogels and subjected to gradually increasing pressure modulated by the increase in ventilator tidal volume (Fig. 2J). The hydrogel burst was monitored by aqueous submersion and PASCO Capstone software. The pure MeTro hydrogel burst after a pressure of 2.8 ± 0.07 kPa, whereas MeTro/SN hydrogels containing 1 and 1.5% (w/v) SN burst at 3.6 ± 0.10 and 3.7 ± 0.12 kPa, respectively (Fig. 2K). The pleural defects that were sealed with the engineered nanocomposites of 1 and 1.5% (w/v) SN experienced mostly higher burst pressure compared with those treated with commercial sealants including Evicel $(1.4 \pm 0.36 \text{ kPa})$, Coseal $(2.5 \pm 0.37 \text{ kPa})$, and Progel $(2.2 \pm 0.47 \text{ kPa})$ as well as sutured lung tissue (1.8 \pm 0.54 kPa) (Fig. 2K).

MeTro/SN hydrogels exhibit fast in vitro hemostasis

Injuries and surgical procedures are often plagued by physiologically disruptive blood loss, so the biomaterials used to treat them must ideally facilitate hemostasis. Thus, the in vitro hemostatic performance of MeTro/SN hydrogels as well as the commercial cellulosebased hemostat Surgicel was assessed using fresh human whole blood (Fig. 3A). Untreated blood (control) that was activated with calcium chloride started to form a clot after 15 ± 0.83 min (Fig. 3B). Blood was also treated with polymerized MeTro/SN hydrogels, which exhibited decreased clotting time at SN concentrations of 1 or 1.5% (w/v). Whole blood treated with the pure MeTro hydrogel clotted in 14 ± 0.53 min, whereas the use of MeTro/SN hydrogels with 1 or 1.5% (w/v) SN decreased clotting time to $12 \pm 0.38 \min (P < 0.01)$ or $11 \pm 0.29 \text{ min } (P < 0.001)$, respectively, which was comparable to that of Surgicel (12 \pm 0.53 min, P < 0.01) (Fig. 3B). Within 16 min of treatment, the blood was fully clotted for the latter two samples, as indicated by their increase in clot weight compared with the untreated control (Fig. 3C) as well as through hemoglobin absorbance assays, which marked an increase in hemoglobin density in the forming clots (Fig. 3D). The MeTro/SN hydrogels appeared to promote hemostasis without causing hemolysis, as indicated by the hemolysis ratio of $20 \pm 1.6\%$, which was far less than the 50% maximum permitted for medical application and was not different between the hydrogel formulations (Fig. 3E) (38). To analyze the effect of SNs on blood clotting, we incubated pure MeTro and MeTro/SN containing 1% (w/v) SN hydrogels in DPBS and measured the zeta potential of the solution over time (fig. S8). Because the surface charge of the solution incubated with MeTro/SN was consistently lower than that of MeTro, we theorized that anionic SNs could leach out of the composite hydrogel and readily interact with blood cells to promote clotting (fig. S8).

We further evaluated the hemostatic properties of the MeTro/SN materials by conducting a coagulation factor XII (FXII) activation assay. As confirmed through zeta potential measurements, an SN has a high density of negatively charged silanol groups on its surface that can electrostatically interact with the positively charged amino acid residues on FXII (39) as well as adsorb intrinsic pathway factors that activate prothrombin and FX (40). These interactions may facilitate the activation of FXII, thereby accelerating the coagulation cascade and promoting hemostasis (41). We observed that the FXIIa activity in the pure MeTro hydrogel (7.96 \pm 3.10 plasma equivalent units/dl) increased significantly in the presence of 1.5% (w/v) SN (71.6 \pm 26.7 plasma equivalent units/dl) (P < 0.05) (fig. S9). The negligible FXIIa activity at low SN concentrations suggests that the hydrogel matrix alone did not activate FXII.

MeTro/SN hydrogels exhibit in vitro biocompatibility

Hemostatic biomaterial-based sealants that are intended for prolonged use in the body must be biocompatible to avoid immune shock or complications with recovery. In vitro cytocompatibility assays were thus conducted using hLFB cells that were seeded on the surface of polymerized MeTro or MeTro/SN hydrogels. Representative images at 1 and 7 days of culture based on live/dead assay or cytoskeleton (actin) and nuclear staining [4',6-diamidino-2-phenylindole dihydrochloride (DAPI)] showed that hLFBs maintained viability, spreading, and proliferation through 7 days of incubation (Fig. 3, F and G). The blue signal in the actin/DAPI staining of the MeTro/SN hydrogel after 1 day of hLFB seeding may be attributed to the nonspecific binding of fluorescent dyes with SNs, which disappeared by day 7 because SNs could be dispelled from the hydrogel surface. The viability of cells seeded onto MeTro (97 \pm 0.72%) or MeTro/SN with 1% (w/v) SN (98 \pm 0.69%) was comparable to that of cells that were seeded on the well plate (control) (98 \pm 0.18%) after 5 (fig. S10) or 7 days of culture (Fig. 3H). The cell number increased from day 1 to day 7 in all samples (Fig. 3I). Furthermore, a PrestoBlue assay was conducted to monitor cell viability as measured by metabolic activity. The enzymatic activity in viable cells reduces resazurin to fluorescent resorufin. The RFU (relative fluorescence unit) of resorufin produced by the control cells was higher than that of hLFB cells seeded on MeTro or MeTro/SN hydrogels. The resorufin RFU also increased in each individual sample throughout the incubation period, indicating an overall increase in cellular metabolic activity (Fig. 3J).

MeTro/SN hydrogels display in vivo biocompatibility and biodegradability

In vivo biocompatibility and biodegradation of the engineered hydrogels were evaluated through subcutaneous implantation into rat dorsal skin. After 7 and 28 days, the MeTro and MeTro/SN [with 1% (w/v) SN] hydrogels were explanted with surrounding tissue for

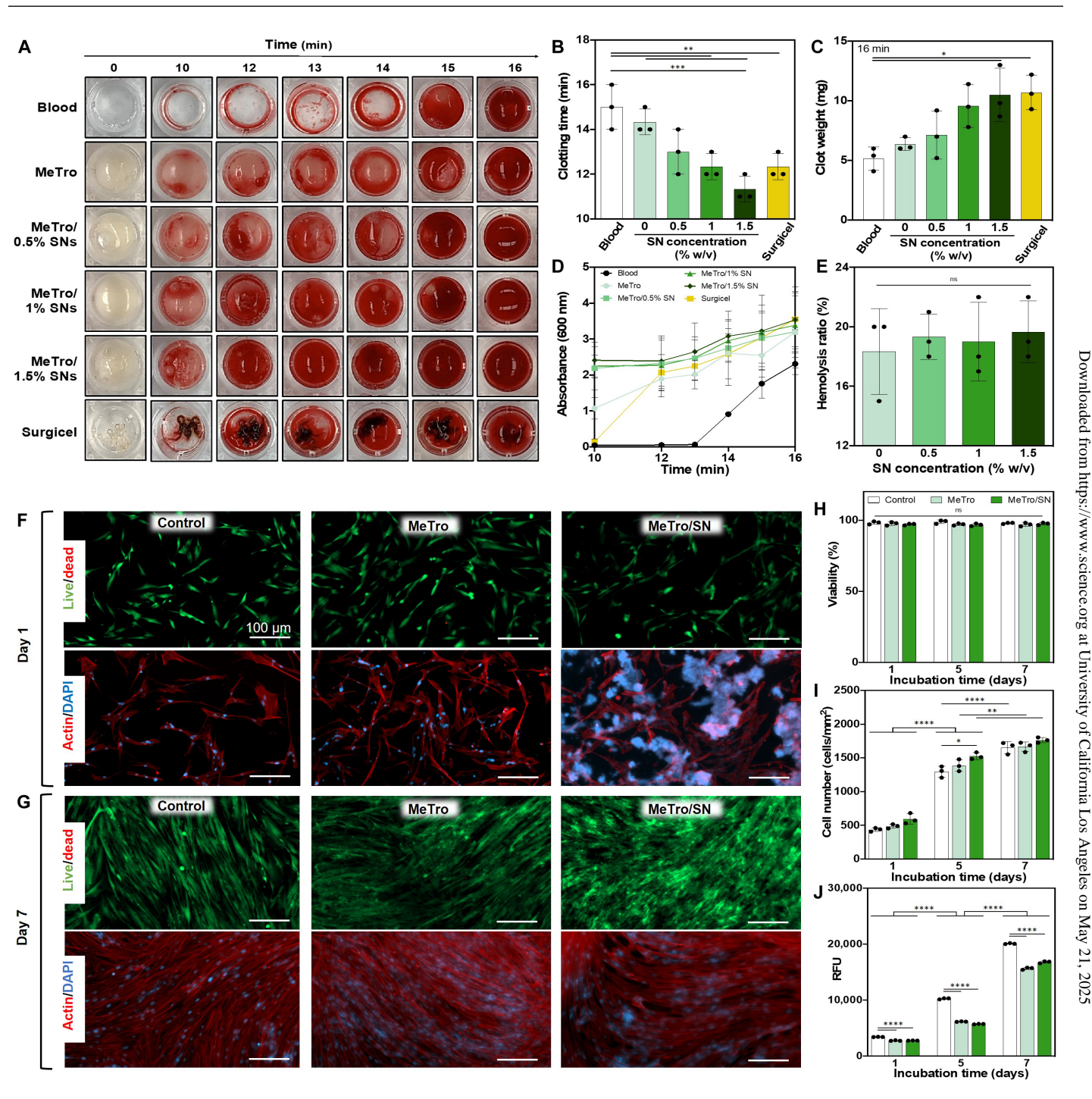


Fig. 3. MeTro/SN hydrogels exhibit faster in vitro hemostasis with higher SN concentrations, and optimized hydrogel formulation retains in vitro biocompatibility. (A) Representative images of clot formation during in vitro hemostatic tests with differing hemostatic sealants. (B) Clotting time of blood with MeTro/SN hydrogels, untreated blood (control), and Surgicel. (C) Quantitative clotted mass measured at 16 min. (D) Absorbance at 600-nm wavelength of lysed clots formed on hydrogels to detect hemoglobin over time. n = 2 or 3. (E) Hemolysis ratio as a function of nanocomposite hydrogel composition. (F and G) Representative live/dead- and actin/DAPI-stained images of hLFB cells 2D seeded on the 24-well plate (control) or the surface of either pure MeTro or MeTro/SN [with 1% (w/v) SN] hydrogels 1 (F) and 7 days (G) postseeding. (H) Quantification of cellular viability over 7 days of 2D culture. (I) Quantification of cell proliferation on the basis of actin/DAPI-stained cell nuclei during 7-day culture. (J) Quantification of metabolic activity using a PrestoBlue assay at days 1, 5, and 7 postseeding. Data in (B) to (E) and (H) to (J) are presented as the means \pm SD; dots represent individual samples. Analysis in (B), (C), and (E) by one-way ANOVA with Tukey's post hoc multiple comparisons test. Analysis in (H) to (J) by two-way ANOVA with Tukey's post hoc multiple comparisons test. In (A) to (C) and (E) to (J), n = 3. ns, not significant; *P < 0.05, **P < 0.01, ***P < 0.001, and ****P < 0.0001. Scale bars, 100 µm.

hematoxylin and eosin (H&E) and immunofluorescence (IF) analysis. Through H&E staining, we noted retention of MeTro/SN to subcutaneous tissue without fibrosis (indicator of a negative host immune response) (Fig. 4A). Healthy cell density and morphology supported the in vivo biocompatibility of the engineered hydrogels. Biodegradation was also noted during the 28-day implantation; the MeTro hydrogel degraded 30 \pm 4.1%, whereas the MeTro/SN nanocomposite degraded $19 \pm 2.2\%$ (P < 0.01) (Fig. 4B). The presence of SNs may have delayed biodegradation of MeTro/SN samples because the hydrogel was reinforced with physical cross-linking, which could have hindered water or enzyme diffusion into the matrix (42). The hydrogel-tissue intersections were also stained for immune markers like macrophages (CD68) and lymphocytes (CD3) (Fig. 4, C and D). Macrophages were present in subcutaneous tissue after 7 days of implantation of either MeTro or MeTro/SN hydrogels; however, there were fewer CD68+ cells identified by day 28 (Fig. 4C). Similarly, there was little lymphocyte infiltration observed in surrounding tissue after 28 days of hydrogel implantation (Fig. 4D). These phenomena implied that there was no long-term negative immune response due to the presence of MeTro or MeTro/SN hydrogels.

MeTro/SN hydrogels effectively seal tissues and achieve hemostasis in vivo using small animal models

Next, we assessed in vivo adhesion and hemostatic performance of the engineered hydrogels in small animals. A rat lung injury model was established where MeTro or MeTro/SN [1% (w/v) SN] prepolymers were photocrosslinked onto an incised and ventilated lung (Fig. 4E). The animals were allowed to recover with the implanted sealant for 7 days before they were euthanized, and the burst pressure of the sealed lungs was measured. The MeTro sealant exhibited a burst pressure of 1.8 \pm 0.09 kPa, whereas the MeTro/SN adhesive burst at 2.3 \pm 0.18 kPa (P < 0.05), similar to the burst pressure of a healthy rat lung (2.2 \pm 0.17 kPa) (Fig. 4E). After 7 days, H&E staining showed that the MeTro/SN sealant remained closely adhered to tissue, and there were no signs of a negative host response (Fig. 4F). Similarly, in IF images, there were very few CD68+ inflammationassociated macrophages in surrounding tissue, supporting the conclusion that the implant did not cause an immune response (Fig. 4G). To further assess the in vivo sealing efficacy of the engineered hydrogels, MeTro or MeTro/SN was used to treat a ruptured artery model in rats wherein the aorta was clamped to restrict blood flow before a needle puncture was performed and sealed by the hydrogels (Fig. 4H). The sealants were left in place for 7 days before the animals were euthanized and burst pressure was measured. The burst pressure of the MeTro-sealed artery was 82 ± 4.5 kPa, whereas that of tissue sealed with MeTro/SN was 98 \pm 3.4 kPa (P < 0.05) (Fig. 4H). Only the nanocomposite hydrogel could withstand a similar pressure to native aorta (100 ± 5.2 kPa), indicating that SN was required to impart physiologically relevant adhesion to seal injured tissues that undergo high distortion forces. Biocompatibility was also noted in tissue surrounding the 7-day MeTro/SN implant because there was no visible fibrosis (Fig. 4I) or macrophage infiltration (Fig. 4J).

In addition to air- and fluid-tight sealing properties, the hemostatic activity of the engineered biomaterials was evaluated through an in vivo tail amputation model conducted in rats. The tail was amputated 6 cm from the tip before the hemostatic hydrogel was applied and cross-linked onto the injury. Blood loss was assessed by collection immediately on filter paper (Fig. 4K). The untreated control

group experienced a blood loss of 3.7 \pm 0.84 mg, whereas treatment with MeTro or MeTro/SN hydrogels resulted in a blood loss of 1.0 \pm 0.07 or 0.33 \pm 0.11 mg, respectively (Fig. 4K). The enhanced hemostatic performance of the MeTro/SN sealant was comparable to treatment with the commercial control Surgicel, which resulted in a blood loss of 0.18 \pm 0.04 mg. Therefore, the engineered hemostatic sealant displayed its potential as a treatment for numerous types of incisional injuries on small animals.

MeTro/SN hydrogels effectively seal and provide hemostasis in vivo using a porcine lung laceration model

Motivated by the successful application of MeTro/SN hydrogels in various small animal models, we further evaluated their biocompatibility and capacity for sealing and hemostasis in larger injuries in a porcine lung laceration model. First, lateral thoracotomy was performed to access the upper lobe of the lung, a 15-mm laceration was prepared, and an air leak was confirmed by the presence of bubbles (Fig. 5, A and B). Then, the engineered hemostatic sealants were applied onto the injury (Fig. 5C). MeTro and MeTro/SN [with 1% (w/v) SN] prepolymers were photocrosslinked over the injury to form hydrogels, whereas Tisseel (control) was in situ polymerized upon application (Fig. 5, D and E). Sealing of the air leak was confirmed by saline submersion of the thoracic cavity (Fig. 5F) and again postoperation using ultrasound imaging to detect signs of pneumothorax caused by air leaking from the lungs into the pleural cavity (Fig. 5G). Given that we observed a hyperechoic pleural line, indicating healthy lung sliding during respiration, as well as A-lines, or horizontal reverberation artifacts of the pleural line, we confirmed that the lungs were adequately sealed without the instance of pneumothorax. After treatment of the lung, pigs were allowed to recover for 14 days during which all animals survived and experienced no signs of wound dehiscence or declining health (as monitored by weight) (fig. S11). After 14 days, the sealed lungs underwent pressure testing using a ventilator both before and after the animals were euthanized. By increasing the tidal volume from 200 ml up to 1000 ml, the pressure in the ventilated lung was increased to the maximum pressure capacity of the lungs (Fig. 5H). In live animals, injured lungs sealed with hydrogels could withstand the same pressure as uninjured pig lungs (760 mmHg or 101 kPa) (Fig. 5I). Hydrogel detachment during this pressure increase was monitored through ultrasound for the occurrence of pneumothorax (Fig. 5J). After animal euthanasia, the thoracic cavity was exposed, and ventilator pressure was again increased to monitor hydrogel detachment from the expanding lungs (Fig. 5K). Once again, both MeTro and MeTro/SN sealants permitted the lungs to withstand the maximum applied pressure.

In addition to air-tight sealing capabilities, the hemostatic activity of the adhesive hydrogels was also tested. Immediately after lung laceration, which caused both a pulmonary air leak and heavy hemorrhage, the pure MeTro hydrogel, MeTro/SN sealant, Tisseel, or Surgicel was applied to the injury before blood loss was measured using filter paper (Fig. 5L). Treatment with MeTro or MeTro/SN sealants resulted in similar, low amounts of blood loss (39 \pm 7.7 or 39 \pm 5.1 mg, respectively) (Fig. 5L). On the other hand, treatment with tissue-adhesive hemostat Tisseel resulted in a blood loss of 63 \pm 8.6 mg, whereas nonadhesive hemostat Surgicel resulted in a loss of 80 \pm 10 mg.

After 14 days of air-tight sealing, IF staining was performed on explanted hydrogels with surrounding lung tissue. The MeTro hydrogel, MeTro/SN sealant, and Tisseel all exhibited adhesion and retention

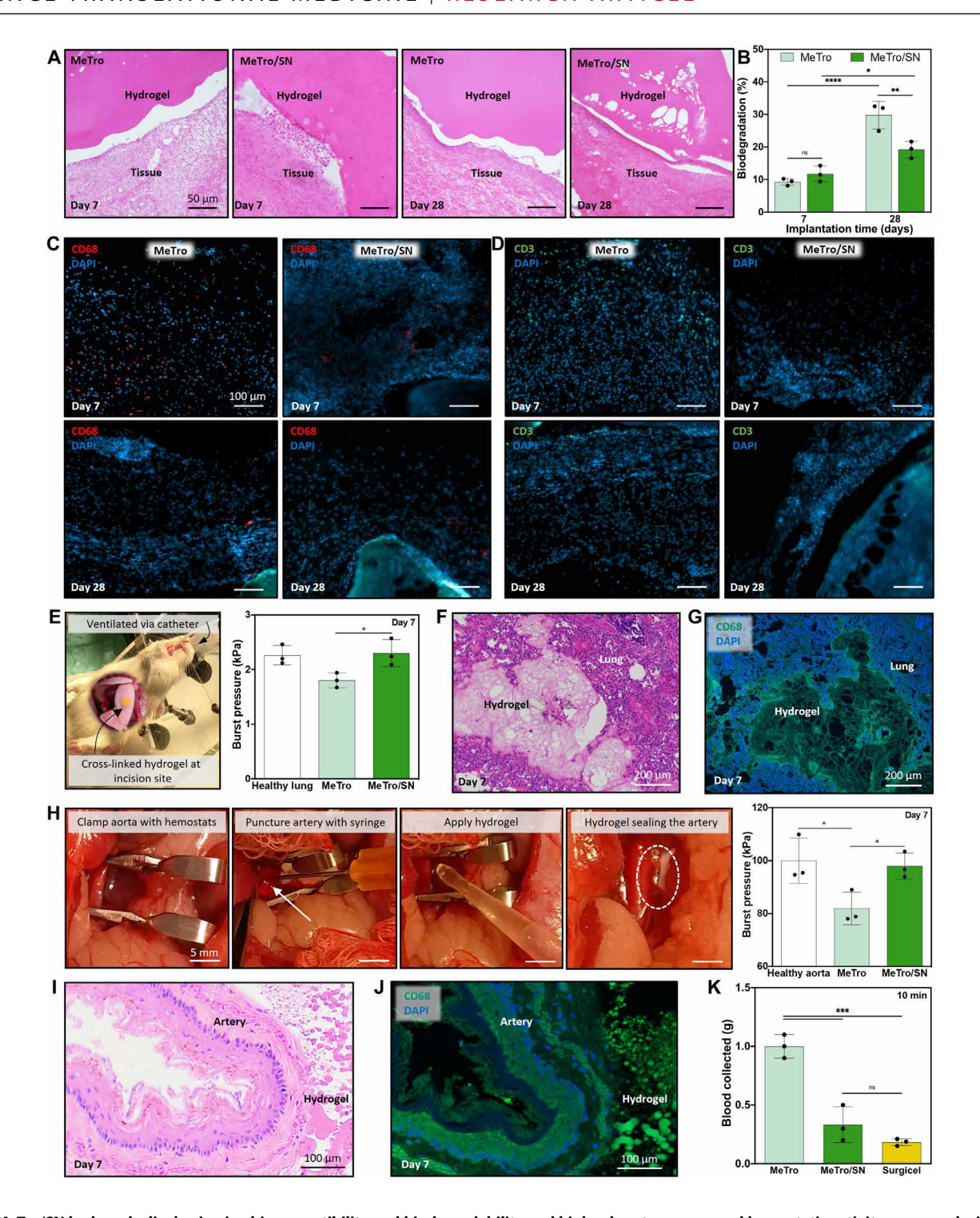


Fig. 4. MeTro/SN hydrogels display in vivo biocompatibility and biodegradability and higher burst pressure and hemostatic activity compared with MeTro in small animal models. (A) H&E staining of hydrogels with surrounding tissue after 7 and 28 days of subcutaneous implantation in rat dorsal skin. MeTro/SN contains 1% (w/v) SN. Scale bar, 50 μ m. (B) In vivo biodegradation of hydrogels. Analysis by two-way ANOVA with Tukey's post hoc multiple comparisons test. (C and D) Immunostaining of either MeTro or MeTro/SN hydrogels with surrounding tissue for macrophages (CD68, red) (C) or lymphocytes (CD3, green) (D). Nuclei were counterstained with DAPI (blue). Scale bar, 100 μ m. (E) Image of model of in vivo sealing evaluation of MeTro and MeTro/SN hydrogels using a rat lung incision model and quantified burst pressure on day 7 postsurgery compared with healthy lung. (F) H&E and (G) IF staining for CD68 (green) and DAPI (blue) on the hydrogel-tissue interface 7 days postsurgery. Scale bars, 200 μ m. (H) In vivo sealing evaluation of the hydrogels using a rat artery incision model and quantified burst pressure compared with healthy aorta. (I) H&E and (J) IF staining for CD68 (green) and DAPI (blue) on the sealed incision site on day 7 postsurgery. Scale bar, 100 μ m. (K) Evaluation of in vivo hemostatic properties by a 6-cm rat tail amputation model. Data in (B), (E), (H), and (K) are presented as the means \pm SD; dots represent individual samples. Analysis in (E), (H), and (K) by one-way ANOVA with Tukey's post hoc multiple comparisons test. In (A) to (K), n = 3. ns, not significant; *P < 0.05, *P < 0.01, *P < 0.001, and *P < 0.001.

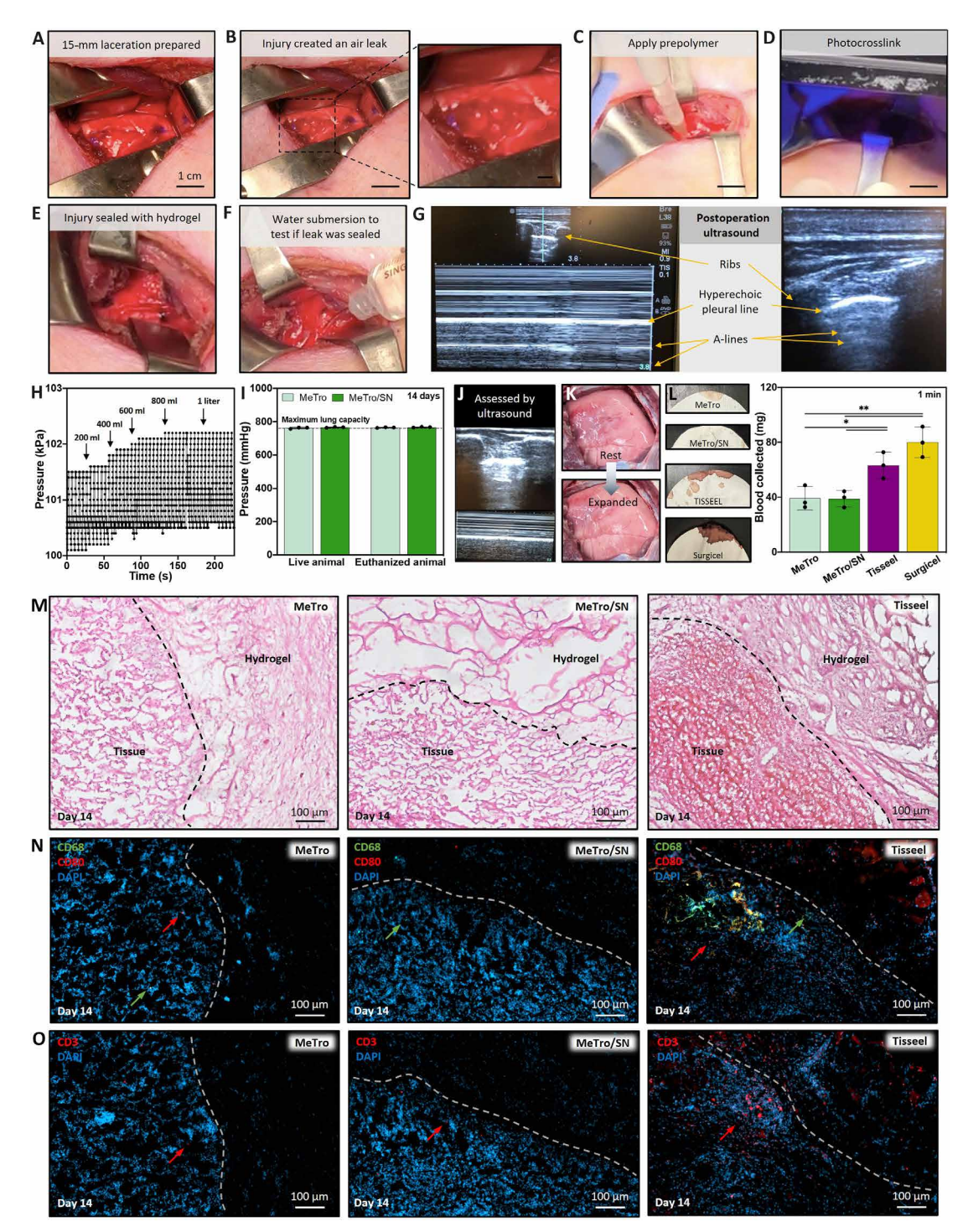


Fig. 5. MeTro/SN hyrogels provide effective in vivo sealing and hemostasis in a porcine lung laceration model. (A to F) Representative images of the in vivo surgical procedure including preparation of a 15-mm laceration on the lung (A), observation of an air leak created by the injury (B), application of MeTro or MeTro/SN [with 1% (w/v) SN] prepolymer (C), photocrosslinking with visible light (D), observation of the injury sealed with hydrogel (E), and confirmation of sealed leak with water submersion test (F). Scale bars, 1 cm. (G) Ultrasound image after surgery showing the location of the ribs and the pleural line. (H) Representative graph depicting the incremental increase in lung pressure during ventilation. (I) Maximum pressure lung sealants could withstand relative to that of healthy lung (dotted line). Analysis by two-way ANOVA with Tukey's post hoc multiple comparisons test. (J) Representative ultrasound image of pig lungs to assess for pneumothorax (hydrogel detachment), while increasing ventilator pressure was applied to live animal. (K) Representative images of lungs at rest and at maximum expansion upon increasing ventilator pressure to euthanized animals. (L) Representative images and average amount of blood collected on filter paper after hemostatic biomaterials were immediately applied on lacerated lung for 1-min hemostatic test. Analysis by one-way ANOVA with Tukey's post hoc multiple comparisons test. (M) H&E staining of the explanted hydrogel and tissue samples on day 14 postsurgery where dashes indicate approximate boundaries. (N and O) IF staining for CD68 (green), CD80 (red), and DAPI (blue) (N) or for CD3 (red) and DAPI (blue) (O) on the incision site 14 days postsurgery. Data are presented as the means ± SD; dots represent individual samples. n = 3. *P < 0.05 and **P < 0.05 and **P < 0.01.

on the lung tissue, as confirmed by H&E staining (Fig. 5M). Tissue surrounding the MeTro and MeTro/SN hydrogels had appropriate morphology and density and did not appear to have fibrosis. Furthermore, there was cell infiltration into the engineered MeTro and MeTro/SN hydrogels, which could be promising for tissue regeneration (fig. S12). On the other hand, tissue near Tisseel showed signs of inflammation or fibrosis, as seen by the overgrown network of cells (Fig. 5M) (43). This fibrotic behavior could be a result of diffusive constraints of the fibrin sealant that hindered the flow of nutrients and the ingrowth of fibroblasts (44). Immune activity was further characterized by fluorescence staining for inflammation-associated biomarkers such as active macrophages (CD80), pan-macrophages (CD68) (Fig. 5N), and lymphocytes (CD3) (Fig. 5O). After 14 days of implantation, there was little immune response visible in the lung tissue adjacent to either MeTro or MeTro/SN sealants. There was very little presence of active macrophages (those directly associated with the inflammatory response) (Fig. 5N) and lymphocytes (Fig. 5O) in tissue near the MeTro and MeTro/SN hydrogels. On the contrary, there was notable infiltration of both immune markers in the tissue near the commercial sealant Tisseel, which was in accordance with the fibrosis observed in histology (Fig. 5M). In conclusion, the flexible, hemostatic, and adhesive MeTro/SN hydrogel was able to provide air-tight sealing of a bleeding injury without inducing an abnormal immune response.

DISCUSSION

Our nanocomposite hydrogel-based hemostatic sealant was engineered to overcome the limitations that often accompany current methods of surgical treatment of hemorrhagic soft tissue injuries. Ideal treatments for such inflictions involve a hemostatic agent combined with a sealing material that can biodegrade as the wound regenerates. However, there are limited surgical materials that provide combined characteristics of appropriate mechanical properties, strong wet tissue adhesion, biocompatibility, and effective hemostasis. Therefore, we engineered MeTro/SN nanocomposites to be an easy-to-use wound sealing platform suitable for soft and elastic organ injuries.

Appropriate mechanical properties are essential for hydrogel applications in dynamic tissues; therefore, we first optimized the composition of the MeTro/SN sealant through mechanical testing. To be compatible with dynamic soft tissues, we sought to engineer a hydrogel with a Young's modulus in the range of 0.1 to 200 kPa (45). Many surgical sealants rely on polymers or proteins such as poly(ethylene glycol) (Coseal), bovine serum albumin (BioGlue), and fibrin (Tisseel) to provide a strong matrix. BioGlue has a Young's modulus of 3.1 MPa, 30-fold higher than that of either Coseal or Tisseel, making the hydrogel very stiff and nonstretchable (46). Gelatin-based sealants have been investigated to treat soft ruptured tissues, but they tend to have a relatively low Young's modulus (47). On the other hand, synthetic polymers like polyacrylic acid (PAA) have been used to make strong hydrogels, and although they can enhance the Young's modulus of the gel (48), they also reduce its flexibility (49). Inorganic compounds like GO have also been incorporated into hydrogels to tune their mechanical and thermal properties (50). Tensile tests confirmed that GO promoted matrix cohesion even under high stress and strain. However, synthetic polymers are often not biodegradable, which increases the risk of cytotoxicity (51), and inorganic components are known to induce DNA damage (52). Our previous work on a UVcrosslinked MeTro lung sealant exhibited more hysteresis, as seen

through the higher energy loss after cyclic compression (35%) (22) compared with that of the MeTro/SN hemostatic sealant in this study (14%). We also engineered elastic hydrogel adhesives using MeTro and GelMA and observed that although adding MeTro enhanced the extensibility of the composite, it also compromised the Young's modulus (4 kPa), which was lower than that of many soft tissues (19). Another MeTro/GelMA composite that was designed for peripheral nerve repair exhibited a Young's modulus of 15 kPa, which is much lower than that of native neural tissues (20, 53). Herein, the mechanical properties of our MeTro/SN hydrogel were improved from previous formulations and were also within the range of native soft tissues such as lungs (54) and arteries (55), and its conductivity was within the range of native cardiovascular tissue (0.005 to 0.16 S/m) (56) and the nervous system (0.08 to 1.3 S/m) (57).

The MeTro/SN hydrogels also depicted robust adhesion on various types of tissues. Many surgical sealants like Evicel, Coseal, and Progel exhibit low tissue adhesion properties, which may limit their utility on elastic or dynamic organs. Other synthetic sealants such as cyanoacrylate-based Dermabond have high adhesion strength (710 kPa to rat skin) (58) but also high mechanical stiffness (which can encumber normal tissue movement) (59) and cytotoxicity (from polymerization and degradation by-products) (60), both of which may limit their clinical translation. Prior literature has also reported bioadhesive hydrogels for wound closure based on a blend of natural (gelatin and alginate) and synthetic (PAA and polyacrylamide) polymers that exhibited strong in vitro adhesion in the range of 120 to 400 kPa but weaker adhesion under conditions that mimicked body fluids (phosphate-buffered saline and cysteine) (61, 62). To enhance wet tissue adhesion, catechol-containing compounds have been used to repel the hydration layer on tissue surfaces and interact with surface moieties (63). For instance, hydrogels containing polydopaminegrafted carbon nanotubes displayed an adhesion strength of 60 kPa even at varying temperatures or duration of application (64); however, the inorganic nanomaterials can exhibit cytotoxicity (65). Mussel adhesive proteins were also used to enable an adhesion strength of 150 kPa from a hyaluronic acid hydrogel; however, they caused lower cell viability compared with untreated control cells (66). Even our MeTro lung sealant with a similar methacrylation degree exhibited an in vitro adhesion strength of 54 kPa (22), whereas an antibacterial peptide-containing MeTro and GelMA gel exhibited a strength of 45 kPa (19). Herein, our MeTro/SN nanocomposite displayed robust adhesion mediated by electrostatic, hydrogen, covalent, and ionic bonding interactions with tissue surfaces.

In addition to enhancing tissue adhesion, increasing the SN concentration within MeTro/SN hydrogels correlated with enhanced hemostatic activity. Clay minerals such as SN enact hemostasis primarily by engaging with and aggregating red blood cells through their high water absorbance capacity, unique nanopore structures, hydrophilic and zwitterionic surfaces that enable electrostatic interactions with blood (67), and their enhancement of hydrogel adhesion to produce a physical barrier on the wound site (30). Furthermore, hydrogels absorbed clotting factors from the blood, whereas the electronegative surface of SN promoted the binding of Hageman factor (or coagulation FXII), activating the intrinsic coagulation cascade (68). As a result, hydrogels containing hemostatic clays like kaolin or Laponite had reduced blood clotting time (28, 34, 69-71). For example, GO-containing hydrogels infused with kaolin exhibited high water absorption, which could bolster the innate hemostatic properties of GO, but high kaolin

concentrations resulted in lower cell viability (69). Polyvinyl alcohol and alginate hydrogels incorporated Laponite to decrease clotting time, but they had high mechanical properties (Young's modulus of 300 to 1000 kPa) (34) that were unsuitable for soft and elastic tissues such as lungs (1 to 5 kPa) and vascular tissue (10 to 100 kPa) (54, 55). Herein, the MeTro/SN hydrogels enacted rapid hemostasis without compromising mechanical strength, biocompatibility, or other essential properties required for tissue regeneration.

MeTro/SN hydrogels showcased their simultaneous adhesive and hemostatic abilities during in vivo assessments. Many commercial hemostats such as Surgicel or ferric sulfate-based Quick-Stat do not have mechanisms in place for tissue adhesion. Other hemostats like BioGlue exhibit an adhesion strength of 35 kPa (72), but the hightensile Young's modulus (3.1 MPa) (46) could be too stiff to seal injuries on elastic organs like lungs. Our lab previously developed soft and elastic GelMA sealants that sealed in vivo rat lung defects so that the sealed lungs could withstand the same pressure as uninjured lungs (73). We also noted the in vivo hemostatic properties of GelMA sealants on rat liver punctures where the sealant caused 40% less blood loss compared with the untreated injury (control) (11). Hemostatic efficacy was enhanced to 50% less blood loss than the control for dopamine-modified and iron-chelated GelMA or GelMAC-Fe (11). Dopamine-grafted chitosan and zinc ions produced hemostatic wound dressings that decreased blood loss by 90% after rat tail amputation (74). Another hemostatic hydrogel containing tannic acid stopped 80% of blood loss after rat liver puncture (75). Gelatin (28) or PAA/carboxymethylcellulose (76) hydrogels containing Laponite also reduced blood loss after liver hemorrhage compared with the untreated injury. Herein, the MeTro/SN hydrogels exemplified their two-pronged approach to establish hemostasis and tissue sealing for the treatment of hemorrhagic tissue injuries. Blood loss after tail amputation was decreased by 99% (compared with control), and physiologically relevant adhesion was observed even after long-term in vivo implantation. Potent hemostatic properties often increase the risk of system thrombosis, but we did not notice any such effects during in vivo experiments. This was likely because of the key safety measures we implemented such as using low SN concentrations and embedding the nanoclay in a hydrophilic polymer matrix that not only engaged in chemical/physical interactions with SN but also promoted strong tissue adhesion that could further prevent SNs dislodging into the bloodstream (40, 77).

The hemostatic sealant was also tested on porcine lung injuries where it effectively minimized blood loss and provided prolonged, air-tight sealing of the lacerated lung. We also noted a negligible immune response to the MeTro/SN hydrogel, which correlated with prior reports on the minimal cytotoxic effects of Laponite at concentrations ranging from 2% (w/v) (78) to 10% (w/v) (79). Laponite can biodegrade into nontoxic ions, such as Na⁺, Mg²⁺, Li⁺, and Si(OH)₄, that have the potential to enhance bone tissue regeneration by modulating specific differentiation processes (80). We previously tested the sealing ability of GelMA (73) or MeTro (22) on pig lung pleural defects. The GelMA sealant effectively sealed the air leak up to 14 days without signs of pneumothorax, but there was notable macrophage infiltration in tissue surrounding the hydrogel (73). MeTro displayed similar sealing efficacy with less macrophage activation compared with the GelMA-treated tissue (22). Furthermore, both sealants required UV light for cross-linking, which can cause photocarcinogenesis and other biosafety concerns (81). The sealing ability of a dextran and chitosan hydrogel on sheep lung parenchymal injury was comparable to that of BioGlue, but its ability to withstand dynamic pressure conditions was not adequately assessed through increasing pressure tests, nor was its hemostatic efficacy or cytocompatibility evaluated (43). Herein, the MeTro/SN hemostatic sealant was appropriately evaluated for all claimed applications (hemostasis, tissue adhesion, and biocompatibility) and proved to be more effective compared with commercial competitors in such regard.

Although Tisseel, MeTro, and MeTro/SN hydrogels displayed similar sealing abilities on porcine lung injuries, it is important to consider the distinct risks associated with the use of fibrin-based sealants like Tisseel, including potential allergic reactions or transmission of infectious agents, that necessitate careful consideration in their clinical application (82). In comparison, the MeTro/SN hydrogel presented notable advantages. Its composition not only ensured reliable sealing of wounds but also actively contributed to the healing process. Because tropoelastin is a soluble precursor of elastin, it plays a role in cell signaling in numerous tissue structures, which indirectly mediates angiogenesis (23, 83). Furthermore, the MeTro/SN hydrogel acted as a scaffold for cell regrowth, thereby promoting wound closure in the areas surrounding the injury. Such characteristics are particularly beneficial in biomedical applications where tissue regeneration is crucial. In addition, the ease of application and the controllability in the delivery of MeTro/SN make it a user-friendly option in surgical settings, ultimately enhancing its practicality and effectiveness. These attributes highlight the potential of the MeTro/SN hydrogel as a superior alternative in certain clinical scenarios and also underscores the importance of tailored approaches in surgical wound management. Ultimately, we showcased the potential of MeTro/SN hydrogels for clinical translation as hemostatic sealants for ruptured soft tissues.

Although this study demonstrates the strong potential of the MeTro/SN hydrogel as an effective hemostatic sealant, certain limitations should be considered. The in vivo degradation profile of the hydrogel has not been fully characterized over extended periods, and further studies are needed to understand its breakdown products and long-term biocompatibility. In addition, although the hydrogel has shown strong adhesion and hemostatic properties, its performance with high-pressure vascular injuries and in minimally invasive procedures, such as laparoscopic or robotic-assisted surgeries where precise application and adhesion under restricted access conditions are critical, remains to be fully evaluated. The efficacy of this material in patients with coagulopathy or those on anticoagulant therapy also requires further investigation to determine its suitability for a broader patient population. Another consideration is the biodistribution and clearance of SNs, because long-term accumulation could pose safety concerns, necessitating further studies to confirm their systemic impact. Although the hydrogel's tunability offers promising opportunities for patient-specific formulations, additional research is required to optimize its properties for different tissue types and injury severities. Last, the large-scale production and cost-effectiveness of MeTro/SN hydrogels have not yet been assessed, which will be essential for ensuring their practical translation into clinical settings. These limitations do not diminish the significance of this study but highlight key areas for future research to further enhance the hydrogel's safety, efficacy, and clinical applicability.

MATERIALS AND METHODS

Study design

This study characterizes and evaluates the performance of a hemostatic sealant based on MeTro and SNs for the rapid and effective closure of ruptured soft tissues. Physical, adhesion, in vitro hemostatic efficacy, in vitro cell, and in vivo tests on rats and pigs were conducted to assess the safety and efficacy of the engineered MeTro/ SN sealant. The in vivo rat experiments were approved by the University of California, Los Angeles (UCLA) Animal Research Committee protocol ARC-2021-113, and the in vivo pig experiments were approved by the Institutional Animal Care and Use Committee protocol S22108 at the University of California, San Diego. Sample sizes were determined on the basis of prior literature to ensure statistically significant results while minimizing the number of animals used in accordance with ethical guidelines. Experiments were replicated thrice to ensure reproducibility, and sample sizes for each study are reported in the figure legends. For in vivo studies, animals were randomly assigned to experimental groups to reduce selection bias. Blinding was applied during outcome analysis, with investigators analyzing histological, hemostatic, and adhesion-related outcomes blinded to treatment conditions. Data collection was stopped once prespecified end points were reached, including mechanical failure, clot formation, adhesion strength thresholds, hemostatic performance, or predefined survival periods in vivo. Data inclusion criteria required samples to meet experimental conditions without visible contamination or procedural errors, and exclusion criteria involved incomplete datasets, procedural inconsistencies, or abnormal physiological responses unrelated to the hydrogel. Outliers, identified visually using a quartile-quartile (Q-Q) plot and statistically using either a Shapiro-Wilk test or Kolmogorov-Smirnov test (for n > 3) where the significance level was defined as $\alpha = 0.05$, were evaluated for experimental errors. If they were due to methodological inconsistencies, they were excluded, whereas biologically relevant variations were retained. Standard guidelines have been followed to provide sufficient information detailing the methods used in this work, and a Materials Design Analysis Reporting Checklist has been provided.

Materials

MeTro was synthesized using human recombinant tropoelastin (University of Sydney). SNs (or Laponite-XLG XR) were purchased from BYK Additives. MA, paraformaldehyde, Triton X-100, and bovine serum albumin were purchased from Sigma-Aldrich. DPBS, PrestoBlue reagent, deuterated dimethyl sulfoxide, and Slide-A-Lyzer MINI were purchased from Thermo Fisher Scientific. hLFB cells (CC2512) were purchased from Lonza Bioscience. Anti-CD68, anti-CD3, and anti-CD80 antibodies were purchased from Abcam. Dulbecco's modified Eagle's medium was purchased from American Type Culture Collection, fetal bovine serum (FBS) was from Corning, and penicillin/streptomycin was from Life Technologies. Commercial live/dead kits, Alexa Fluor 594 (phalloidin), and DAPI were purchased from Invitrogen. Mayer's hematoxylin was purchased from Electron Microscopy Sciences. Polypropylene sutures were purchased from Ad Surgical.

Synthesis of MeTro and fabrication of MeTro/SN hydrogels

MeTro was synthesized by adding 15% (v/v) MA into a 10% (w/v) solution of tropoelastin prepared in Milli-Q water. This reaction was performed at 4°C for 16 hours. The solutions were diluted and

dialyzed with distilled water (Slide-A-Lyzer MINI; molecular weight cutoff, 35 kDa) at 4°C for 7 days to remove the excess MA and MA by-products. After dialysis, the solution was frozen at -80°C for 24 hours, lyophilized, and stored at 4°C. To prepare MeTro/SN hydrogels, we first dissolved 15% (w/v) MeTro and either 0, 0.5, 1, or 1.5% (w/v) SN in 0.03% (w/v) LAP solution prepared in Milli-Q water. Then, the prepolymer solution was photocrosslinked with visible light (100 mW/cm², 395 to 405 nm) with an exposure time of 80 s.

Mechanical characterization

The mechanical properties of MeTro/SN hydrogels were characterized through tensile and compression tests. For tensile tests, the prepolymers were photocrosslinked in rectangular polydimethylsiloxane molds (length: 12 mm; width: 5 mm; depth: 1 mm) using visible light for 80 s. The hydrogels were then secured in tape and loaded into a mechanical tester (Instron 5943) where they were stretched until failure at a strain rate of 1 mm/min. Data were collected using Bluehill Universal software where ultimate strength and extensibility were directly reported, Young's modulus was calculated as the initial slope of the stress-versus-strain curve from 0 to 20% strain (84, 85), and toughness was quantified as the area under the stressversus-strain curve. For compression tests, the prepolymers were cross-linked in cylindrical polydimethylsiloxane molds (diameter: 5 mm; height: 3 mm) using visible light for 80 s. The hydrogels were loaded into the Instron mechanical tester and compressed until failure at a rate of 1 mm/min. The compression modulus was calculated as the initial slope of the stress-versus-strain curve (from 0 to 20% strain) using the data collected on Bluehill Universal software. For cyclic compression testing, the cylindrical hydrogels compressed until 50% strain at a rate of 1 mm/min and then relaxed until 0% strain at the same rate for five cycles. The energy loss was calculated using the last cycle as the difference between the area under the loading and unloading curves.

In vitro hemostatic activity

In vitro hemostatic activity of MeTro/SN was assessed using fresh whole human (Zen-Bio Inc.) blood that was inoculated with 3.6% (w/v) sodium citrate to prevent premature clotting. The citrated blood was activated with 0.3 M calcium chloride (9:1 ratio) to initiate coagulation after 10 s of vortexing. Simultaneously, all formulations of MeTro/SN hydrogels were prepared at the bottom of 48-well plates. The activated blood was pipetted on top of the hydrogels, and at predetermined time points, the wells were washed with 0.9% (w/v) saline solution to halt the clotting process. The liquid was aspirated and washed repeatedly until the solution was clear to ensure the removal of soluble blood components. After the trial of time points was complete, the clotting time was determined on the basis of the observation of a visible clot, and the hemoglobin concentration was measured by lysing the clots and measuring the absorbance at 600 nm. In addition, clots were dried and weighed to determine the clot mass with respect to clotting time.

In vivo sealing efficacy using a rat lung incision model

The rat lung incision test was performed under protocol ARC-2021-113 at UCLA. Male Wistar rats (200 to 250 g) were purchased from Charles River Laboratories. Spontaneous respiration of the rats was assessed after inhalable anesthesia was introduced. Under general anesthesia, animals were quickly intubated by mouth (in less than a minute) using a catheter guidewire as a guide for an endotracheal

tube. Afterward, the endotracheal tube of the animals was connected to the ventilation system. The skin on the ventral thorax was shaved and disinfected. Lateral thoracotomy was performed on the right side, and the thorax was incised (2 cm) laterally at the position of the third intercostal space. Next, the underlying pectoral muscles were dissected to expose the ribs and intercostal muscles, so that intercostal spaces 3 to 5 were accessible. The intercostal muscles in the intercostal space were incised, starting about 3 mm from the edge of the sternum (to avoid injury to the internal thoracic arteries, which passed behind the sternocostal joints) and continuing sideways for about 1 to 1.5 cm. Blunt-ended surgical scissors were inserted through the third intercostal space, passing under the sternum and emerging through the third intercostal space on the other side of the sternum while slightly raising the rib cage. Raising the rib cage was necessary to prevent injury to major vessels and to access the pleural cavity and lung to make the surgical incision. After lateral thoracotomy, a wound retractor was placed and the operating field around the lung was draped with filter paper. A standardized lung incision (2 mm) was prepared with a surgical blade. After the application of the MeTro or MeTro/SN [with 1% (w/v) SN] hydrogels, a thoracic catheter was placed as a chest tube to remove chest air during closure (chest tube was removed before recovery). The thoracic wound was anatomically closed with polypropylene sutures (4-0 and 5-0) by closing the intercostal space and the skin separately. The intercostal space was closed by suturing the adjacent rips together. To prevent postoperative pneumothorax, the skin incision was set one intercostal space caudal from the thoracotomy. Furthermore, the lung was gently inflated during the final closure of the thorax. Rats were euthanized 7 days postsurgery to assess the durability and biocompatibility of the hydrogels. Some hydrogels were explanted with surrounding tissue for H&E and IF analysis using previously described methods. For some euthanized animals, the ex vivo burst pressure of the hydrogel sealants was measured using a syringe pump.

In vivo sealing and hemostatic efficacy using a pig lung incision model

The pig lung incision test was performed under Institutional Animal Care and Use Committee protocol S22108 at the University of California, San Diego, using adult Yorkshire pigs (male or female). After sterile surgical preparation and induction of general anesthesia, a 4- to 6-cm lateral chest incision was created, and thoracotomy was performed to access the pleural space. Right thoracotomy was performed at the fourth intercostal space using the muscle-sparing thoracotomy technique. A laceration of 15 mm in length and about 3 mm in depth was made with a surgical scalpel, and an air leak was confirmed by bubble formation in the expelled blood. The animals were placed on short periods of apnea (15 to 30 s), while either MeTro, MeTro/SN [with 1% (w/v) SN], or commercial hemostatic sealant Tisseel was cross-linked on top of the injury. Hemostatic efficacy was assessed through a 1-min hemostatic test wherein blood loss was measured on preweighed filter paper after biomaterial treatment. Air-tight sealing was confirmed by saline submersion of the thoracic cavity through the lack of bubble formation after inflation of the lung with a pressure of 15 to 25 cmH₂O. The thoracic wound was then anatomically closed with polypropylene sutures (3-0) by closing the intercostal space and the skin separately. To prevent a postoperative pneumothorax, the skin incision was set one intercostal space (fifth) caudal from the thoracotomy. Furthermore, the lungs were gently inflated during the final closure of the thorax. The

animals were extubated, and the thoracostomy tube, which was placed into the right pleural space percutaneously before the closure of the surgical incision and was secured posteriorly to a one-way Heimlich valve, was removed postoperatively. The skin was completely closed with an absorbable monofilament subcuticular suture. After the operation, thoracic ultrasound was performed to evaluate for any radiographic signs of pneumothorax. Ultrasound gel was applied to both left and right sides of the thorax. Lungs were evaluated for healthy lung sliding, B-lines, comet tail artifacts, and A-lines. A linear surface ultrasound probe was used to assess for the presence of lung sliding bilaterally.

After 14 days of treatment of the lung laceration with the hemostatic hydrogel-based sealants, the sealing efficacy and biocompatibility of the hydrogels were evaluated. Before animal euthanasia, the tidal volume was increased to build ventilator pressure in the intubated lungs. Ultrasound was performed simultaneously to assess for pneumothorax amid the increasing pressure, ultimately denoting the sealing efficacy of the implanted hydrogels. After the animals were euthanized, thoracotomy was performed to expose the lacerated region before another pressure test was conducted on the sealed lungs. Hydrogel detachment due to high pressure was observed by saline submersion, and pressure data were recorded using PASCO Capstone software. Then, the lung tissue samples treated with either MeTro, MeTro/SN, or Tisseel were explanted for IF analysis.

Statistical analysis

Statistical analysis of all numerical data was carried out using GraphPad Prism software (version 8). Data are presented as the means \pm SD. Data normality was tested using both visual methods, such as a Q-Q plot, and statistical methods, including Shapiro-Wilk test and Kolmogorov-Smirnov test. Unpaired two-tailed Student's t test was performed for analysis of two groups, and an analysis of variance (ANOVA) test followed by Tukey's post hoc test for multiple comparisons was performed for multiple-group analysis. A oneway ANOVA was performed to analyze the effect of one independent variable upon a dependent variable, whereas a two-way ANOVA was conducted when there were two independent variables. The differences between groups were considered to be statistically significant at *P < 0.05, **P < 0.01, ***P < 0.001, and ****P < 0.0001. All individual-level data are available in data file S1.

Supplementary Materials

The PDF file includes:

Materials and Methods Figs. S1 to S12 Legend for data file S1

 ${\bf Other\ Supplementary\ Material\ for\ this\ manuscript\ includes\ the\ following:}$

Data file S1

MDAR Reproducibility Checklist

REFERENCES AND NOTES

- N. Annabi, A. Tamayol, S. R. Shin, A. M. Ghaemmaghami, N. A. Peppas, A. Khademhosseini, Surgical materials: Current challenges and nano-enabled solutions. *Nanotoday* 9, 574–589 (2014)
- P. Ferreira, R. Pereira, J. F. J. Coelho, A. F. M. Silva, M. H. Gil, Modification of the biopolymer castor oil with free isocyanate groups to be applied as bioadhesive. *Int. J. Biol. Macromol.* 40, 144–152 (2007).
- C. Oliveira, C. Santos, F. Bezerra, M. Bezerra, L. Rodrigues, Utilization of cyanoacrylates adhesives in skin suture. Rev. Bras Cir. Plást. 25. 573–576 (2010).

SCIENCE TRANSLATIONAL MEDICINE | RESEARCH ARTICLE

- A. C. Morani, J. F. Platt, A. J. Thomas, R. K. Kaza, M. M. Al-Hawary, R. H. Cohan, I. R. Francis, K. M. Elsayes, Hemostatic agents and tissue sealants: Potential mimics of abdominal abnormalities. *Am. J. Roentgenol.* 211, 760–766 (2018).
- L. Sanders, J. Nagatomi, Clinical applications of surgical adhesives and sealants. Crit. Rev. Biomed. Eng. 42, 271–292 (2014).
- M. C. Oz, J. F. Rondinone, N. S. Shargill, FloSeal Matrix: New generation topical hemostatic sealant. J. Card. Surg. 18, 486–493 (2003).
- X. Xie, J. K. Tian, F. Q. Lv, R. Wu, W. B. Tang, Y. K. Luo, Y. Q. Huang, J. Tang, A novel hemostatic sealant composed of gelatin, transglutaminase and thrombin effectively controls liver trauma-induced bleeding in dogs. *Acta Pharmacol. Sin.* 34, 983–988 (2013).
- 8. A. J. Singer, H. C. Thode Jr., A review of the literature on octylcyanoacrylate tissue adhesive. *Am. J. Surg.* **187**, 238–248 (2004).
- L. Montanaro, C. R. Arciola, E. Cenni, G. Ciapetti, F. Savioli, F. Filippini, L. A. Barsanti, Cytotoxicity, blood compatibility and antimicrobial activity of two cyanoacrylate glues for surgical use. *Biomaterials* 22, 59–66 (2000).
- D. H. Sierra, A. W. Eberhardt, J. E. Lemons, Failure characteristics of multiple-component fibrin-based adhesives. J. Biomed. Mater. Res. 59, 1–11 (2002).
- S. Baghdasarian, B. Saleh, A. Baidya, H. Kim, M. Ghovvati, E. S. Sani, R. Haghniaz, S. Madhu, M. Kanelli, I. Noshadi, N. Annabi, Engineering a naturally derived hemostatic sealant for sealing internal organs. *Mater. Today Bio* 13, 100199 (2022).
- M. Ghovvati, S. Baghdasarian, A. Baidya, J. Dhal, N. Annabi, Engineering a highly elastic bioadhesive for sealing soft and dynamic tissues. *J. Biomed. Mater. Res. B Appl. Biomater.* 110, 1511–1522 (2022).
- W. R. Ranger, D. Halpin, A. S. Sawhney, M. Lyman, J. Locicero, Pneumostasis of experimental air leaks with a new photopolymerized synthetic tissue sealant. *Am. Surg.* 63, 788–795 (1997).
- M. S. Allen, D. E. Wood, R. W. Hawkinson, D. H. Harpole, R. J. McKenna, G. L. Walsh, E. Vallieres, D. L. Miller, F. C. Nichols, W. R. Smythe, R. D. Davis, Prospective randomized study evaluating a biodegradable polymeric sealant for sealing intraoperative air leaks that occur during pulmonary resection. *Ann. Thorac. Surg.* 77, 1792–1801 (2004).
- C. Fuller, Reduction of intraoperative air leaks with Progel in pulmonary resection: A comprehensive review. J. Cardiothorac. Surg. 8, 90 (2013).
- N. Annabi, S. R. Shin, A. Tamayol, M. Miscuglio, M. A. Bakooshli, A. Assmann,
 P. Mostafalu, J.-Y. Sun, S. Mithieux, L. Cheung, X. Tang, A. S. Weiss, A. Khademhosseini,
 Highly elastic and conductive human-based protein hybrid hydrogels. *Adv. Mater.* 28, 40–49 (2016).
- J. Rnjak-Kovacina, S. G. Wise, Z. Li, P. K. M. Maitz, C. J. Young, Y. Wang, A. S. Weiss, Tailoring the porosity and pore size of electrospun synthetic human elastin scaffolds for dermal tissue engineering. *Biomaterials* 32, 6729–6736 (2011).
- S. Lee, E. S. Sani, A. R. Spencer, Y. Guan, A. S. Weiss, N. Annabi, Human-recombinant-Elastin-based bioinks for 3D bioprinting of vascularized soft tissues. *Adv. Mater.* 32, e2003915 (2020).
- N. Annabi, D. Rana, E. S. Sani, R. Portillo-Lara, J. L. Gifford, M. M. Fares, S. M. Mithieux, A. S. Weiss, Engineering a sprayable and elastic hydrogel adhesive with antimicrobial properties for wound healing. *Biomaterials* 139, 229–243 (2017).
- J. R. Soucy, E. Shirzaei Sani, R. Portillo Lara, D. Diaz, F. Dias, A. S. Weiss, A. N. Koppes, R. A. Koppes, N. Annabi, Photocrosslinkable gelatin/tropoelastin hydrogel adhesives for peripheral nerve repair. *Tissue Eng. Part A* 24, 1393–1405 (2018).
- N. Annabi, K. Tsang, S. M. Mithieux, M. Nikkhah, A. Ameri, A. Khademhosseini, A. S. Weiss, Highly elastic micropatterned hydrogel for engineering functional cardiac tissue. *Adv. Funct. Mater.* 23, 4950–4959 (2013).
- N. Annabi, Y.-N. Zhang, A. Assmann, E. S. Sani, G. Cheng, A. D. Lassaletta, A. Vegh,
 B. Dehghani, G. U. Ruiz-Esparza, X. Wang, S. Gangadharan, A. S. Weiss, A. Khademhosseini,
 Engineering a highly elastic human protein–based sealant for surgical applications. Sci.
 Transl. Med. 9, eaai7466 (2017).
- S. G. Wise, G. C. Yeo, M. A. Hiob, J. Rnjak-Kovacina, D. L. Kaplan, M. K. Ng, A. S. Weiss, Tropoelastin: A versatile, bioactive assembly module. *Acta Biomater.* 10, 1532–1541 (2014).
- C. Cha, S. R. Shin, N. Annabi, M. R. Dokmeci, A. Khademhosseini, Carbon-based nanomaterials: Multifunctional materials for biomedical engineering. ACS Nano 7, 2891–2897 (2013).
- A. K. Gaharwar, N. A. Peppas, A. Khademhosseini, Nanocomposite hydrogels for biomedical applications. *Biotechnol. Bioeng.* 111, 441–453 (2014).
- S. E. Baker, A. M. Sawvel, N. Zheng, G. D. Stucky, Controlling bioprocesses with inorganic surfaces: Layered clay hemostatic agents. *Chem. Mater.* 19, 4390–4392 (2007).
- R. K. Avery, H. Albadawi, M. Akbari, Y. S. Zhang, M. J. Duggan, D. V. Sahani, B. D. Olsen, A. Khademhosseini, R. Oklu, An injectable shear-thinning biomaterial for endovascular embolization. *Sci. Transl. Med.* 8, 365ra156 (2016).
- A. K. Gaharwar, R. K. Avery, A. Assmann, A. Paul, G. H. McKinley, A. Khademhosseini,
 D. Olsen, Shear-thinning nanocomposite hydrogels for the treatment of hemorrhage.
 ACS Nano 8, 9833–9842 (2014).
- 29. US Food and Drug Administration, "Obsidio 510 (k) approval letter" (FDA, 2022).

- Y. Yang, X. Wang, F. Yang, B. Mu, A. Wang, Progress and future prospects of hemostatic materials based on nanostructured clay minerals. *Biomater. Sci.* 11, 7469–7488 (2023).
- S. R. U. Rehman, R. Augustine, A. A. Zahid, R. Ahmed, M. Tariq, A. Hasan, Reduced graphene oxide incorporated GelMA hydrogel promotes angiogenesis for wound healing applications. *Int. J. Nanomedicine* 14, 9603–9617 (2019).
- A. K. Nguyen, P. L. Goering, V. Reipa, R. J. Narayan, Toxicity and photosensitizing assessment of gelatin methacryloyl-based hydrogels photoinitiated with lithium phenyl-2, 4, 6-trimethylbenzoylphosphinate in human primary renal proximal tubule epithelial cells. *Biointerphases* 14, 021007 (2019).
- C. Nomicisio, M. Ruggeri, E. Bianchi, B. Vigani, C. Valentino, C. Aguzzi, C. Viseras, S. Rossi, G. Sandri, Natural and synthetic clay minerals in the pharmaceutical and biomedical fields. *Pharmaceutics* 15, 1368 (2023).
- N. Golafshan, R. Rezahasani, M. T. Esfahani, M. Kharaziha, S. Khorasani, Nanohybrid hydrogels of laponite: PVA-alginate as a potential wound healing material. *Carbohydr. Polym.* 176, 392–401 (2017).
- C.-E. Brunchi, S. Morariu, Laponite—from dispersion to gel—structure, properties, and applications. *Molecules* 29, 2823 (2024).
- S. T. Stealey, A. K. Gaharwar, S. P. Zustiak, Laponite-based nanocomposite hydrogels for drug delivery applications. *Pharmaceuticals* 16, 821 (2023).
- Z. Zhao, G. D. Spyropoulos, C. Cea, J. N. Gelinas, D. Khodagholy, Ionic communication for implantable bioelectronics. Sci. Adv. 8. eabm7851 (2022).
- C. Zhou, Z. Yi, Blood-compatibility of polyurethane/liquid crystal composite membranes. Biomaterials 20, 2093–2099 (1999).
- Y. Guo, M. Wang, Q. Liu, G. Liu, S. Wang, J. Li, Recent advances in the medical applications of hemostatic materials. *Theranostics* 13, 161–196 (2023).
- 40. V. Gryshchuk, N. Galagan, Silica nanoparticles effects on blood coagulation proteins and platelets. *Biochem. Res. Int.* **2016**, 2959414 (2016).
- 41. A. H. Schmaier, The elusive physiologic role of factor XII. J. Clin. Invest. 118, 3006–3009 (2008).
- S. Sharifi, S. B. Blanquer, T. G. van Kooten, D. W. Grijpma, Biodegradable nanocomposite hydrogel structures with enhanced mechanical properties prepared by photocrosslinking solutions of poly (trimethylene carbonate)–poly (ethylene glycol)–poly (trimethylene carbonate) macromonomers and nanoclay particles. *Acta Biomater.* 8, 4233–4243 (2012).
- B. Balakrishnan, U. Payanam, A. Laurent, M. Wassef, A. Jayakrishnan, Efficacy evaluation of an in situ forming tissue adhesive hydrogel as sealant for lung and vascular injury. *Biomed. Mater.* 16, 044106 (2021).
- W. D. Spotnitz, Fibrin sealant: The only approved hemostat, sealant, and adhesive—A laboratory and clinical perspective. *ISRN Surg.* 2014, 203943 (2014).
- A. Wahlsten, A. Stracuzzi, I. Lüchtefeld, G. Restivo, N. Lindenblatt, C. Giampietro,
 A. E. Ehret, E. Mazza, Multiscale mechanical analysis of the elastic modulus of skin. *Acta Biomater.* 170, 155–168 (2023).
- A. N. Azadani, P. B. Matthews, L. Ge, Y. Shen, C.-S. Jhun, T. S. Guy, E. E. Tseng, Mechanical properties of surgical glues used in aortic root replacement. *Ann. Thorac. Surg.* 87, 1154–1160 (2009).
- Y. Lee, J. W. Bae, J. W. Lee, W. Suh, K. D. Park, Enzyme-catalyzed in situ forming gelatin hydrogels as bioactive wound dressings: Effects of fibroblast delivery on wound healing efficacy. J. Mater. Chem. B 2, 7712–7718 (2014).
- R. Chapla, M. Alhaj Abed, J. West, Modulating functionalized poly (ethylene glycol) diacrylate hydrogel mechanical properties through competitive crosslinking mechanics for soft tissue applications. *Polymers* 12, 3000 (2020).
- V. R. Feig, H. Tran, M. Lee, Z. Bao, Mechanically tunable conductive interpenetrating network hydrogels that mimic the elastic moduli of biological tissue. *Nat. Commun.* 9, 2740 (2018).
- 50. J. Shen, B. Yan, T. Li, Y. Long, N. Li, M. Ye, Mechanical, thermal and swelling properties of poly (acrylic acid)–graphene oxide composite hydrogels. *Soft Matter* **8**, 1831–1836 (2012).
- R. Mihai, I. Florescu, V. Coroiu, A. Oancea, M. Lungu, In vitro biocompatibility testing of some synthetic polymers used for the achievement of nervous conduits. *J. Med. Life* 4, 250–255 (2011).
- S. Gurunathan, M.-H. Kang, M. Jeyaraj, J.-H. Kim, Differential cytotoxicity of different sizes of graphene oxide nanoparticles in leydig (TM3) and sertoli (TM4) cells. *Nanomaterials* 9, 139 (2019).
- T. Rickett, Z. Amoozgar, W. Sun, Y. Yeo, R. Shi, "A photo-crosslinkable chitosan hydrogel for peripheral nerve anastomosis," in 2009 2nd International Conference on Biomedical Engineering and Informatics (IEEE, 2009), pp. 1–5.
- S. R. Polio, A. N. Kundu, C. E. Dougan, N. P. Birch, D. E. Aurian-Blajeni, J. D. Schiffman, A. J. Crosby, S. R. Peyton, Cross-platform mechanical characterization of lung tissue. *PLOS ONE* 13, e0204765 (2018).
- N. K. Awad, H. Niu, U. Ali, Y. S. Morsi, T. Lin, Electrospun fibrous scaffolds for smalldiameter blood vessels: A review. Membranes 8, 15 (2018).
- M. Ghovvati, K. Bolouri, L. Guo, N. Kaneko, X. Jin, Y. Xu, Z. Hua, Y. Lei, Harnessing the power of electroconductive polymers for breakthroughs in tissue engineering and regenerative medicine. *Mater. Chem. Horizons* 2, 195–206 (2023).

SCIENCE TRANSLATIONAL MEDICINE | RESEARCH ARTICLE

- M. Ghovvati, L. Guo, K. Bolouri, N. Kaneko, Advances in electroconductive polymers for biomedical sector: Structure and properties. *Mater. Chem. Horizons* 2, 125–137 (2023).
- M. Chen, Y. Wu, B. Chen, A. M. Tucker, A. Jagota, S. Yang, Fast, strong, and reversible adhesives with dynamic covalent bonds for potential use in wound dressing. *Proc. Natl. Acad. Sci. U.S.A.* 119, e2203074119 (2022).
- J. M. Korde, B. Kandasubramanian, Biocompatible alkyl cyanoacrylates and their derivatives as bio-adhesives. *Biomater. Sci.* 6, 1691–1711 (2018).
- G. Pascual, S. Sotomayor, M. Rodríguez, B. Pérez-Köhler, A. Kühnhardt, M. Fernández-Gutiérrez, J. San Román, J. M. Bellón, Cytotoxicity of cyanoacrylate-based tissue adhesives and short-term preclinical in vivo biocompatibility in abdominal hernia repair. PLOS ONE 11, e0157920 (2016).
- H. Yuk, C. E. Varela, C. S. Nabzdyk, X. Mao, R. F. Padera, E. T. Roche, X. Zhao, Dry double-sided tape for adhesion of wet tissues and devices. *Nature* 575, 169–174 (2019).
- H. Yang, C. Li, J. Tang, Z. Suo, Strong and degradable adhesion of hydrogels. ACS Appl. Bio Mater. 2, 1781–1786 (2019).
- W.-Y. Quan, Z. Hu, H.-Z. Liu, Q.-Q. Ouyang, D.-Y. Zhang, S.-D. Li, P.-W. Li, Z.-M. Yang, Mussel-inspired catechol-functionalized hydrogels and their medical applications. *Molecules* 24, 2586 (2019).
- L. Han, K. Liu, M. Wang, K. Wang, L. Fang, H. Chen, J. Zhou, X. Lu, Mussel-inspired adhesive and conductive hydrogel with long-lasting moisture and extreme temperature tolerance. *Adv. Funct. Mater.* 28, 1704195 (2018).
- M. V. Kharlamova, C. Kramberger, Cytotoxicity of carbon nanotubes, graphene, fullerenes, and dots. Nanomaterials 13, 1458 (2023).
- E. Y. Jeon, J. Lee, B. J. Kim, K. I. Joo, K. H. Kim, G. Lim, H. J. Cha, Bio-inspired swellable hydrogel-forming double-layered adhesive microneedle protein patch for regenerative internal/external surgical closure. *Biomaterials* 222, 119439 (2019).
- C. G. Velopulos, N. Y. Enwerem, A. Obirieze, X. Hui, Z. G. Hashmi, V. K. Scott,
 E. E. Cornwell III, E. B. Schneider, A. H. Haider, National cost of trauma care by payer status.
 J. Surg. Res. 184, 444–449 (2013).
- L. Jiang, Y. Li, Y. Li, C. Guo, Y. Yu, Y. Zou, Y. Yang, Y. Yu, J. Duan, W. Geng, Q. Li, Z. Sun, Silica nanoparticles induced the pre-thrombotic state in rats via activation of coagulation factor XII and the JNK-NF-κB/AP-1 pathway. *Toxicol. Res.* 4, 1453–1464 (2015).
- Y. Liang, C. Xu, G. Li, T. Liu, J. F. Liang, X. Wang, Graphene-kaolin composite sponge for rapid and riskless hemostasis. Colloids Surf. B Biointerfaces 169, 168–175 (2018).
- Y.-H. Cheng, S.-J. Cheng, H.-H. Chen, W.-C. Hsu, Development of injectable graphene oxide/laponite/gelatin hydrogel containing Wharton's jelly mesenchymal stem cells for treatment of oxidative stress-damaged cardiomyocytes. *Colloids Surf. B Biointerfaces* 209, 112150 (2022)
- C. Xu, P. Xu, Y. Gao, F. Gao, X. Zhuang, H. Zhang, X. Dong, Hierarchically cross-linked gelatin/tannic acid/laponite hybrid antimicrobial hydrogel for hemostatic dressings. *Comp. Commun.* 43, 101743 (2023).
- L. X. Chen, M. Coulombe, F. Barthelat, A. Rammal, L. Mongeau, K. Kost, Investigation of surgical adhesives for vocal fold wound closure. *Laryngoscope* 129, 2139–2146 (2019).
- A. Assmann, A. Vegh, M. Ghasemi-Rad, S. Bagherifard, G. Cheng, E. S. Sani, G. U. Ruiz-Esparza, I. Noshadi, A. D. Lassaletta, S. Gangadharan, A. Tamayol, A. Khademhosseini, N. Annabi, A highly adhesive and naturally derived sealant. *Biomaterials* 140, 115–127 (2017).
- Y. Yang, Y. Liang, J. Chen, X. Duan, B. Guo, Mussel-inspired adhesive antioxidant antibacterial hemostatic composite hydrogel wound dressing via photo-polymerization for infected skin wound healing. *Bioact. Mater.* 8, 341–354 (2022).
- X. Shao, X. Yang, Y. Zhou, Q. Xia, Y. Lu, X. Yan, C. Chen, T. Zheng, L. Zhang, Y. Ma, Antibacterial, wearable, transparent tannic acid–thioctic acid–phytic acid hydrogel for adhesive bandages. Soft Matter 18, 2814–2828 (2022).
- L. Xu, G. Jiao, Y. Huang, P. Ren, M. Liang, D. Wei, T. Zhang, Laponite nanoparticlecrosslinked carboxymethyl cellulose-based injectable hydrogels with efficient

- underwater-specific adhesion for rapid hemostasis. *Int. J. Biol. Macromol.* **255**, 128288 (2024).
- C. Li, C. Mu, W. Lin, T. Ngai, Gelatin effects on the physicochemical and hemocompatible properties of gelatin/PAAm/laponite nanocomposite hydrogels. ACS Appl. Mater. Interfaces 7, 18732–18741 (2015).
- J. W. Davern, L. Hipwood, L. J. Bray, C. Meinert, T. J. Klein, Addition of Laponite to gelatin methacryloyl bioinks improves the rheological properties and printability to create mechanically tailorable cell culture matrices. APL Bioeng. 8, 016101 (2024).
- J. Li, Z. Tian, H. Yang, L. Duan, Y. Liu, Infiltration of laponite: An effective approach to improve the mechanical properties and thermostability of collagen hydrogel. *J. Appl. Polym. Sci.* 140, e53366 (2023).
- M. Mousa, J. A. Milan, O. Kelly, J. Doyle, N. D. Evans, R. O. Oreffo, J. I. Dawson, The role of lithium in the osteogenic bioactivity of clay nanoparticles. *Biomater. Sci.* 9, 3150–3161 (2021).
- B. Kozma, M. J. Eide, Photocarcinogenesis: An epidemiologic perspective on ultraviolet light and skin cancer. *Dermatol. Clin.* 32, 301–313 (2014).
- 82. C. Joch, The safety of fibrin sealants. Cardiovasc. Surg. 11, 23-28 (2003).
- A. Al Halawani, L. Abdulkhalek, S. M. Mithieux, A. S. Weiss, Tropoelastin promotes the formation of dense, interconnected endothelial networks. *Biomolecules* 11, 1318 (2021).
- N. Kaneko, M. Ghovvati, Y. Komuro, L. Guo, K. Khatibi, L. L. Ponce Mejia, H. Saber,
 N. Annabi, S. Tateshima, A new aspiration device equipped with a hydro-separator for acute ischemic stroke due to challenging soft and stiff clots. *Interv. Neuroradiol.* 28, 43–49 (2022)
- A. Mostafavi, M. Samandari, M. Karvar, M. Ghovvati, Y. Endo, I. Sinha, N. Annabi,
 A. Tamayol, Colloidal multiscale porous adhesive (bio)inks facilitate scaffold integration.
 Appl. Phys. Rev. 8, 041415 (2021).

Acknowledgments: We would like to thank A. Roy, J. Liu, and S. Mithieux for assistance. Some illustrative schematics were prepared using Biorender.com. Funding: This work was supported by National Institutes of Health (R01-EB023052 and R01-HL140618) to N.A. and National Health and Medical Research Council (GNT1195827) to A.S.W. Rheology work was supported by National Institutes of Health/National Center for Advancing Translational Science UCLA CTSI Grant UL1TR001881 to N.A. Author contributions: N.A. supervised the project. N.A. and A.S.W. conceptualized the work. M.G. and S.J. performed investigative experiments including the in vitro and ex vivo tests. M.G., S.J., N.K., and T.I. designed and conducted the small-animal experiments. S.J., G.Z.C., and J.A.B. designed and conducted the porcine experiments. T.D.M. performed rheological characterization, R.H. conducted the in vitro hemostatic test, M.G. and S.J. analyzed the data, S.J. prepared the schematics, M.G. and S.J. wrote the manuscript, which was reviewed and revised by G.Z.C., N.K., J.A.B., T.I., T.D.M., R.H., R.B.C., A.S.W., and N.A. Competing interests: A.S.W. founded Elastagen Pty Ltd., which was sold to Allergan, an AbbVie company, where A.S.W. has served as a consultant, N.A. cofounded GelMEDIX Inc., holds equity in this company, and has served as a consultant. N.A. and A.S.W. are inventors on patent US9688741B2 for "Elastic hydrogel" assigned to Allergan Australia Pty Ltd., Allergan Pharmaceuticals International Ltd., Harvard College, and Brigham and Women's Hospital Inc. N.A. is an inventor on patent application US11406737B2 for "Gelatin/elastin composites for peripheral nerve repair" assigned to Northeastern University Boston. The other authors declare that they have no competing interests. Data and materials availability: All data associated with this study are present in the paper or the Supplementary Materials.

Submitted 10 July 2024 Resubmitted 16 December 2024 Accepted 21 April 2025 Published 14 May 2025 10.1126/scitranslmed.adr6458